WL-TR-97-4100

FREQUENCY AND MEAN STRESS EFFECTS IN HIGH CYCLE FATIGUE OF Ti-6Al-4V

by

Ryan J. Morrissey

A thesis submitted to the Georgia Institute of Technology
in partial fulfillment of the requirements
for the degree of Master of Science in Mechanical Engineering

Atlanta, Georgia

SEPTEMBER 1997 FINAL REPORT FOR 08/01/96-09/01/97

MATERIALS DIRECTORATE
WRIGHT LABORATORY
AIR FORCE MATERIEL COMMAND
WRIGHT PATTERSON AFB OH 45433-7734

NOTICE

WHEN GOVERNMENT DRAWINGS, SPECIFICATIONS, OR OTHER DATA ARE USED FOR ANY PURPOSE OTHER THAN IN CONNECTION WITH A DEFINITELY GOVERNMENT-RELATED PROCUREMENT, THE UNITED STATES GOVERNMENT INCURS NO RESPONSIBILITY OR ANY OBLIGATION WHATSOEVER. THE FACT THAT THE GOVERNMENT MAY HAVE FORMULATED OR IN ANY WAY SUPPLIED THE SAID DRAWINGS, SPECIFICATIONS, OR OTHER DATA, IS NOT TO BE REGARDED BY IMPLICATION OR OTHERWISE IN ANY MANNER CONSTRUED, AS LICENSING THE HOLDER OR ANY OTHER PERSON OR CORPORATION, OR AS CONVEYING ANY RIGHTS OR PERMISSION TO MANUFACTURE, USE, OR SELL ANY PATENTED INVENTION THAT MAY IN ANY WAY BE RELATED THERETO.

THIS REPORT IS RELEASABLE TO THE NATIONAL TECHNICAL INFORMATION SERVICE (NTIS). AT NTIS, IT WILL BE AVAILABLE TO THE GENERAL PUBLIC, INCLUDING FOREIGN NATIONS.

THIS TECHNICAL REPORT HAS BEEN REVIEWED AND IS APPROVED FOR PUBLICATION.

RYAN MORRISSEY, Project Engineer
Ceramics Development & Materials
Behavior Branch
Metals, Ceramics & NDE Division

GERALD J. PETRAK, Chief
Ceramics Development & Materials
Behavior Branch
Metals, Ceramics & NDE Division

NORMAN M. GEYER, Actg Asst Chief
Metals, Ceramics & NDE Division
Materials Directorate

IF YOUR ADDRESS HAS CHANGED, IF YOU WISH TO BE REMOVED FROM OUR MAILING LIST, OR IF THE ADDRESSEE IS NO LONGER EMPLOYED BY YOUR ORGANIZATION, PLEASE NOTIFY, WL/MLLN, WRIGHT-PATTERSON AFB OH 45433-7817 TO HELP US MAINTAIN A CURRENT MAILING LIST.

COPIES OF THIS REPORT SHOUL.D NOT BE RETURNED UNLESS RETURN IS REQUIRED BY SECURITY CONSIDERATIONS, CONTRACTUAL OBLIGATIONS, OR NOTICE ON A SPECIFIC DOCUMENT.

REPORT DOCUMENTATION PAGE

FORM APPROVED
OMB NO. 0704-0188

1. AGENCY USE ONLY (Leave blank)	2. REPORT DATE	3. REPORT TYPE AND DATES COVERED
	September 1997	Final 08/01/96--09/01/97

4. TITLE AND SUBTITLE
Frequency and Mean Stress Effects in High Cycle Fatigue of Ti-6Al-4V

5. FUNDING NUMBERS
PE 61102F
PR 2310
TA W1
WU 23

6. AUTHOR(S)
Ryan Morrissey

7. PERFORMING ORGANIZATION NAMES(S) AND ADDRESS(ES)
WL/MLLN Bldg 655 (Ryan Morrissey)
2230 Tenth St Ste 1
Wright-Patterson AFB OH 45433-7817

8. PERFORMING ORGANIZATION REPORT NUMBER

9. SPONSORING/MONITORING AGENCY NAMES(ES) AND ADDRESS(ES)
MATERIALS DIRECTORATE
WRIGHT LABORATORY
AIR FORCE MATERIEL COMMAND
WRIGHT PATTERSON AFB OH 45433-7734
POC: RYAN J. MORRISSEY, WL/MLLN (937) 255-1348

10. SPONSORING/MONITORING AGENCY REPORT NUMBER
WL-TR-97-4100

11. SUPPLEMENTARY NOTES

12a. DISTRIBUTION/AVAILABILITY STATEMENT
Approved for public release; distribution unlimited

12b. DISTRIBUTION CODE

13. ABSTRACT (Maximum 200 words)
The objective of this project was to extend past research on fatigue of Ti-6Al-4V into conditions which more closely reflect actual use conditions. This included testing at a range of frequencies (70, 400, 1800 Hz) to determine the effect of frequency on the fatigue strength. In addition, testing was performed at various stress ratios (0.1, 0.5, 0.8) to determine the effects of mean stress on the HCF performance of Ti-6Al-4V. This included an examination of the effects of cyclic and time-dependent strain accumulation on the fracture mode at high mean stresses.
Frequench effects weere observed at low stress ratios, resulting in higher fatigue strengths as the frequency increased. Possible causes include strain rate effects on dislocation motion, loss of active primary slip systems at high frequencies in hexagonal close-packed and body-centered cubic materials, and environmental damage. Results obtained at high mean stress show that the behavior of Ti-6Al-4V consists of a complex combination of fatigue, cyclic creep, and strain ratchetting. Fractographic analysis combined with cyclic creep studies were used to further define the mechanisms which led to the observed behavior.

14. SUBJECT TERMS	15. NUMBER OF PAGES
modeling, computer simulation, binary systems, thermodynamic data base	87
	16. PRICE CODE

17. SECURITY CLASSIFICATION OF REPORT	18. SECURITY CLASSIFICATION OF THIS PAGE	19. SECURITY CLASSIFICATION OF ABSTRACT	20. LIMITATION OF ABSTRACT
UNCLASSIFIED	UNCLASSIFIED	UNCLASSIFIED	SAR

ACKNOWLEDGMENT

I would like to recognize my advisors, Dr. David L. McDowell and Dr. Ted Nicholas, and thank them for support and guidance that they offered me throughout this endeavor. I would also like to thank Dr. Richard W. Neu and Dr. W. S. Johnson for agreeing to serve as committee members and lending their expertise to this project.

The experiments were conducted at the Materials Behavior Branch (WL/MLLN), in the Materials Directorate of Wright Laboratories at Wright-Patterson AFB, OH with the help and support of many Air Force and University of Dayton Research Institute personnel. Special thanks are extended to Rick Goodman and Ken Goecke for their help in conducting this research.

I would also like to thank the Air Force Palace Knight Program, which has given me this opportunity.

My final expression of appreciation and gratitude is to my family, and especially my wife Chrystal, for her overwhelming support and encouragement. Her belief in me has been an invaluable asset not only in this project but in every aspect of my life.

TABLE OF CONTENTS

LIST OF TABLES

LIST OF FIGURES

SUMMARY

Titanium alloys have been widely used in the aircraft industry, especially for engine applications. A high percentage of blades and discs found in cold sections of jet engines today are composed almost exclusively of various titanium alloys. Due to its popularity and many practical applications, the majority of the HCF research performed on titanium alloys has centered on Ti-6Al-4V. Most of this data has been collected at low stress ratios (-1.0, 0.1) and at low frequencies (30-50 Hz). In contrast, engine airfoils can experience short bursts of low-amplitude fatigue at a high mean stress (corresponding to a high stress ratio) at frequencies much greater than 1 kHz. Since most HCF data on titanium has been obtained at frequencies and stress ratios which do not reflect in-service conditions, there is a question as to the applicability of this data for design purposes.

The objective of this project was to extend past research into conditions which more closely reflect actual use conditions. This included testing at a range of frequencies (70, 400, and 1800 Hz) to determine the effect of frequency on the fatigue strength. In addition, testing was performed at various stress ratios (0.1, 0.5, 0.8) to determine the effects of mean stress on the HCF performance of Ti-6Al-4V. This included an examination of the effects of cyclic and time-dependent strain accumulation on the fracture mode at high mean stresses.

Frequency effects were observed at low stress ratios, resulting in higher fatigue strengths as the frequency increased. Possible causes include strain rate effects on dislocation motion, loss of active primary slip systems at high frequencies in hexagonal close-packed and body-centered cubic materials, and environmental damage. Results obtained at high mean stress show that the behavior of Ti-6Al-4V consists of a complex combination of fatigue, cyclic creep, and strain ratchetting. Fractographic analysis combined with cyclic creep studies were used to further define the mechanisms which led to the observed behavior.

CHAPTER I

INTRODUCTION

Titanium alloys have been widely used in the aircraft industry, especially for engine applications. Advantages include a very high strength-to-weight ratio, excellent corrosion resistance, and good high temperature properties. A high percentage of blades and discs found in cold sections of jet engines today are composed almost exclusively of various titanium alloys. One of these titanium alloys, the most versatile and the most widely produced, is Ti-6Al-4V.

In the recent past, gas turbine engine designers were primarily concerned with low cycle fatigue (LCF) issues, since most of the military engine failures could be attributed to this phenomenon. This focus led to the development of the Air Force Engine Structural Integrity Program (ENSIP), which has implemented damage tolerant design procedures for all Air Force gas turbine engines [1] and has subsequently reduced the number of LCF failures. As a result, a high percentage of failures now involve high cycle fatigue (HCF). This has led the Air Force to escalate its research activity in this area.

Although there is heightened interest, HCF of titanium alloys has been studied for years. Due to its popularity and many practical applications, Ti-6Al-4V has been the subject of the majority of this research. Most of the HCF data collected thus far for

titanium alloys has been done at low stress ratios ($R_\sigma = \sigma_{min}/\sigma_{max}$ = -1.0, 0.1) and at low frequencies (30-50 Hz). In contrast, engine airfoils can experience short bursts of low-amplitude fatigue at a high mean stress (corresponding to a high stress ratio) at frequencies much greater than 1 kHz. [2] The reason why most tests have been performed at low frequencies can be traced to a lack of equipment necessary to achieve such high loads at high frequency. Since most HCF data on titanium has been obtained at frequencies and stress ratios which do not reflect in-service conditions, there is a question as to the applicability of this data for design purposes.

The goal of this investigation is to extend past research into these areas which have previously been lacking, in an effort to more closely reflect actual use conditions. As was previously mentioned, this includes frequencies on the order of 1 kHz. The majority of testing considered here was performed at 70 and 400 Hz, with some additional testing performed at 1800 Hz. This provides a wide range of frequencies in the appropriate range. In addition, tests at these frequencies were conducted at stress ratios of 0.1, 0.5, and 0.8. This allowed a more in-depth study of the interaction between frequency and mean stress, as well as a look at the effects of high mean loads on the fracture mode.

This study considers just one aspect of the HCF issue, and will be used in conjunction with additional experimental studies currently underway. It is hoped that

eventually the mechanics of the HCF problem can be understood and accounted for in design, instead of relying solely on empirical models.

CHAPTER II

LITERATURE REVIEW

2.1 Overview

Design of components subjected to HCF is generally based on a Goodman Diagram, a plot of stress amplitude versus mean stress for a constant life (such as 10^7 cycles). Whereas the original diagrams attributed to Goodman consist of a straight line connecting the stress amplitude for fully reversed loading on the y-axis to the ultimate stress on the x-axis, a more common procedure is to use experimental data collected for various stress ratios to produce a Modified Goodman Diagram. These diagrams have been used in conjunction with various damage accumulation laws to predict failures under random loading in addition to constant stress amplitude.

Although useful for certain applications, the Goodman Diagram is based on certain assumptions which limit its usefulness. For instance, the diagrams are only valid for the frequency at which the data were obtained, which is generally much lower than the actual frequencies experienced in service conditions. Also, the diagram assumes the same mechanisms are responsible for failure at all stress ratios, which may not be the case. This assumption is important when using linear damage summations laws such as

Miner's Rule to predict a materials response under variable stress amplitudes. Large amounts of bulk damage occurring during cycling at high stress ratios may produce incorrect results when used in conjunction with data from low stress ratios.

This investigation deals with the effects of frequency on the fatigue limit, as well as considering the effects of mean stress on the failure mechanisms in Ti-6Al-4V.

2.2 Frequency Effects

The study of frequency effects on the fatigue properties of metals in laboratory air has not received much attention, and literature on the subject is sparse. This may be due in part to the general belief that frequency has no effect on high cycle fatigue in inert environments, as is certainly the case for many materials, most notably steels. This belief has been perpetuated in introductory fatigue classes and textbooks, which are often based on the fatigue properties of steels. An additional reason has been a lack of equipment necessary to perform high frequency tests.

Literature generally shows that frequency effects are greatest in the HCF regime, which requires specimens to be tested for at least 10^6 cycles. Such tests are not usually feasible since the maximum frequency capacity of most test frames is in the 30-50 Hz range. The development of new high-frequency test frames has been required to perform the necessary tests.

While there have been some studies done on frequency effects, they generally fall into two categories: frequencies on the order of 0.1 - 30 Hz, and ultrasonic frequencies in the vicinity of 20 kHz. In addition, most of these tests were primarily fatigue crack growth tests, did not consider crack initiation, and investigated materials other than titanium alloys.

Studies at the lower frequencies were primarily done in the LCF regime ($< 10^5$ cycles). Tests performed on an aluminum alloy over three orders of magnitude in the low frequency range [3] (0.2 - 20 Hz) have shown an increase in fatigue lives as frequency is increased, although the lives decrease when expressed in terms of time instead of cycles. Another study in the same frequency range [4] produced similar results when testing polycrystalline copper. It was found that low frequencies increased persistent slip band (PSB) formation, while higher frequencies showed greater amounts of hardening and less cyclic plastic strain. In addition, the frequency dependence decreased for higher stress amplitudes and higher frequencies. These tests were performed in laboratory air at room temperature, but most studies in this frequency range involve testing in a corrosive environment. One such study [5] was performed on pure titanium (99.5%) at 450 °C with frequencies ranging from 2 to 20 Hz. Fatigue crack propagation rates were predicted using a constitutive model and compared to experimental results. As was predicted, crack growth rates were strongly frequency dependent, and decreased as frequency increased. In a similar study at high temperatures [6], stainless steels were shown to exhibit a

"critical frequency", above which fatigue crack growth rates were independent of the cyclic frequency. The "critical frequency" was shown to be temperature dependent, and decreased as the temperature decreased. The crack growth rate dependence on frequency was determined to be a result of increased time for oxidation to take place. At the higher frequencies, it was believed that crack propagation proceeded at a faster rate than the oxidation, and hence no frequency effect was seen. Another fatigue crack propagation experiment [7] was performed in a similar frequency range, except aluminum alloys were tested in an aqueous 3.5% NaCl solution. As in the previous experiments, the crack propagation rates increased as frequency decreased. In this study, however, a maximum propagation rate was obtained and further reduction of frequency decreased the rate of propagation. This was not found in the previous studies. The initial increase in propagation rate was explained in a similar manner as the previous studies. The subsequent decrease in propagation rate was explained as a result of repassivation during the long rise time in each load step. The frequency dependence was similar for all three alloys considered, but the magnitudes were found to be alloy dependent. In addition, tests performed in a vacuum showed no frequency effect. It should be noted that all of the previously mentioned experiments were performed at low stress ratios ranging between -1.0 and 0.1.

Ultrasonic tests [8, 9] have been performed under strain control, usually at a stress ratio of -1.0. A definite frequency dependence has been found for steels and various

aluminum and titanium alloys, including Ti-6Al-4V, under these conditions. These materials have shown large increases in fatigue strength as frequencies are increased from the order of 1 Hz to the ultrasonic range.

Research indicates that fatigue of face-centered cubic (FCC) materials is only slightly frequency dependent, whereas fatigue of body-centered cubic (BCC) materials is highly frequency dependent [10]. This has been explained in terms of the dislocation mechanisms of the different structures. At high frequencies, dislocation sources and slip systems remain active for FCC materials, but not for BCC materials.

Frequency effects are normally considered to occur in conjunction with corrosive environments. This may be one reason why little testing has been done on frequency effects in titanium alloys in lab air. However, recent studies [11] have shown laboratory air can be considered a corrosive environment and could be a factor in initiation and propagation of cracks in titanium alloys. Large decreases in fatigue strength and crack propagation resistance have been found for Ti-6Al-4V when tested in laboratory air as compared to a vacuum [12]. The effect seemed to increase in the longer life regime where the stresses are lower.

Crack growth studies in near-α alloys have shown increased growth rates at lower frequencies in air. The effect was attributed to the longer duration of the loading portion of the cycles and not to overall exposure time [13]. This effect could be a factor in reducing fatigue lives at lower frequencies.

2.3 Mean Stress Effects

As was previously mentioned, the effects of frequency at high stress ratios have not been studied comprehensively. Most mean stress studies have been concerned with the change in allowable cyclic amplitudes during constant life tests or the change in fatigue life during constant amplitude tests as the mean stress varies. These tests are used to develop Modified Goodman (or Haigh) Diagrams, which provide engineers a useful tool when designing for HCF. It has been shown [14, 15] that mean stresses can have a significant effect on fatigue life of titanium alloys, and that this effect is texture dependent.

Little has been done concerning the effect of mean stress on the fracture mode of Ti-6Al-4V in HCF, although studies have shown that many materials experience significant progressive plastic deformation at high stress ratios. This is a very important consideration in many HCF applications, specifically in gas turbine engines which can see very high mean stresses during service [2]. Such strain accumulation during fatigue has commonly been referred to as cyclic creep [16-19] or cyclic ratchetting [20-23].

The term cyclic creep is sometimes used to describe plastic strain accumulation which is observed to possess a time-dependent component, usually because the material is known to exhibit creep under static conditions at stress levels similar to those experienced during cycling. Much of this work has been done on copper and other similar alloys.

Cyclic ratchetting, on the other hand, refers to purely time-independent strain accumulation due to the cyclic load in materials which do not tend to exhibit static creep. Strain accumulation in steels has generally been explained in such terms. In many cases, the literature has used these two terms rather interchangeably and somewhat imprecisely. At present there does not seem to be a way to differentiate between these two mechanisms.

Numerous studies have shown [18, 24-28] that Ti-6Al-4V can undergo substantial static creep at room temperature when subjected to stresses as low as 80 percent of the yield stress. Therefore, cycling at high stress ratios means that the material may undergo time-dependent creep.

Creep/fatigue interaction is potentially an important factor in HCF failures, where time dependent deformation (strain accumulation) influences both crack initiation and early growth. This influence is seen by the increased incidence of internal crack initiation and failure [19] in Ti-6Al-4V. Static and cyclic creep tests performed on Ti-6Al-4V specimens [18] with varying microstructure have shown that there is not a one-to-one correspondence between the static and cyclic creep response of the material. These tests seem to indicate that the two processes may be independent and the result of different mechanisms. For some materials, such as copper, the cyclic creep rate has been shown [16, 17] to be greater than the static creep rate. In addition, the cyclic creep tended to promote both initiation and growth of cracks in the material. Loading frequency has also

been found to influence the secondary creep rate [29]. A minimum "secondary creep rate" was found at a frequency close to zero, and the rate increased as the frequency was increased.

One explanation for the increased plastic strain accumulation rates seen in cyclic tests is that part of the deformation is cyclic dependent instead of time dependent and is therefore caused by a different mechanism. Gilmore and Imam [18] have shown that the static and cyclic strain deformation are a result of different mechanisms in Ti-6Al-4V. Cyclic ratchetting may therefore be a contributing, or even the dominant, factor for strain accumulation during HCF in conjunction with creep deformation. Studies have shown that ratchetting can be significant in many materials, most notably steels, when subjected to a high mean stress. Much work has been done recently to explain this phenomenon and model its effects, although not in Ti-6Al-4V. Constitutive models based on a nonlinear dynamic recovery generalization of the kinematic hardening rule of Armstrong and Frederick have recently been used to accurately correlate cyclic strain accumulation under various stress states [20-23].

Cyclic softening has previously been shown to occur in Ti-6Al-4V during HCF due to local stress relaxation [8, 30]. Under load control, this results in increased plastic strain occurring in the specimen. Although this effect was not directly attributed to creep or ratchetting, it does provide a precedence for such behavior in this material.

CHAPTER III

EXPERIMENTAL PROCEDURE

3.1 Material

The material used in this research project was 45 mm diameter Ti-6Al-4V forged bar stock supplied by Teledyne Allvac. The material composition is listed in Table 3-1. It was processed in accordance with ASM 4928L. The material was heat treated at 705°C in a vacuum for two hours followed by a static cool in Argon to below 149 °C. It then received an annealing heat treatment at 549 °C in a vacuum for two hours with a static argon cool to less than 149 °C. This produces a microstructure of wide, plate-like α with intergranular β. As can be seen in Figure 3-1, taken with a Leica 360FE Scanning Electron Microscope, the microstructure is approximately equi-axed in the transverse section, with a slight elongation in the longitudinal section along the longitudinal axis. Grain size for the material was approximately 10 μm. The microstructure contains approximately 90% alpha phase, 10% beta phase as determined by Image-Pro Plus image analysis software. This agrees with the expected results for this material [31]. The α phase consists of a hexagonal close-packed (HCP) crystal structure, while the β phase is BCC.

Displacement controlled tensile tests were performed to determine material properties in the longitudinal direction. The results are shown in Table 3-2, and the stress/strain diagram is shown in Figure 3-2.

Table 3-1. Material Composition

Element	% by Mass	Element	% by Mass
Ti	Balance	Si	0.02
Al	6.41	Mn	0.01
V	4.15	Mo	0.01
O	0.18	N	0.01
Fe	0.16	Zr	0.01
Sn	0.04	H	0.0011
C	0.029	B	0.001
Cr	0.02	Y	0.001
Cu	0.02		

Table 3-2. Material Properties

Yield Strength	990 MPa
Ultimate Strength	1035 MPa
Young's Modulus	109 GPa
Eng. Strain to Failure	19 %

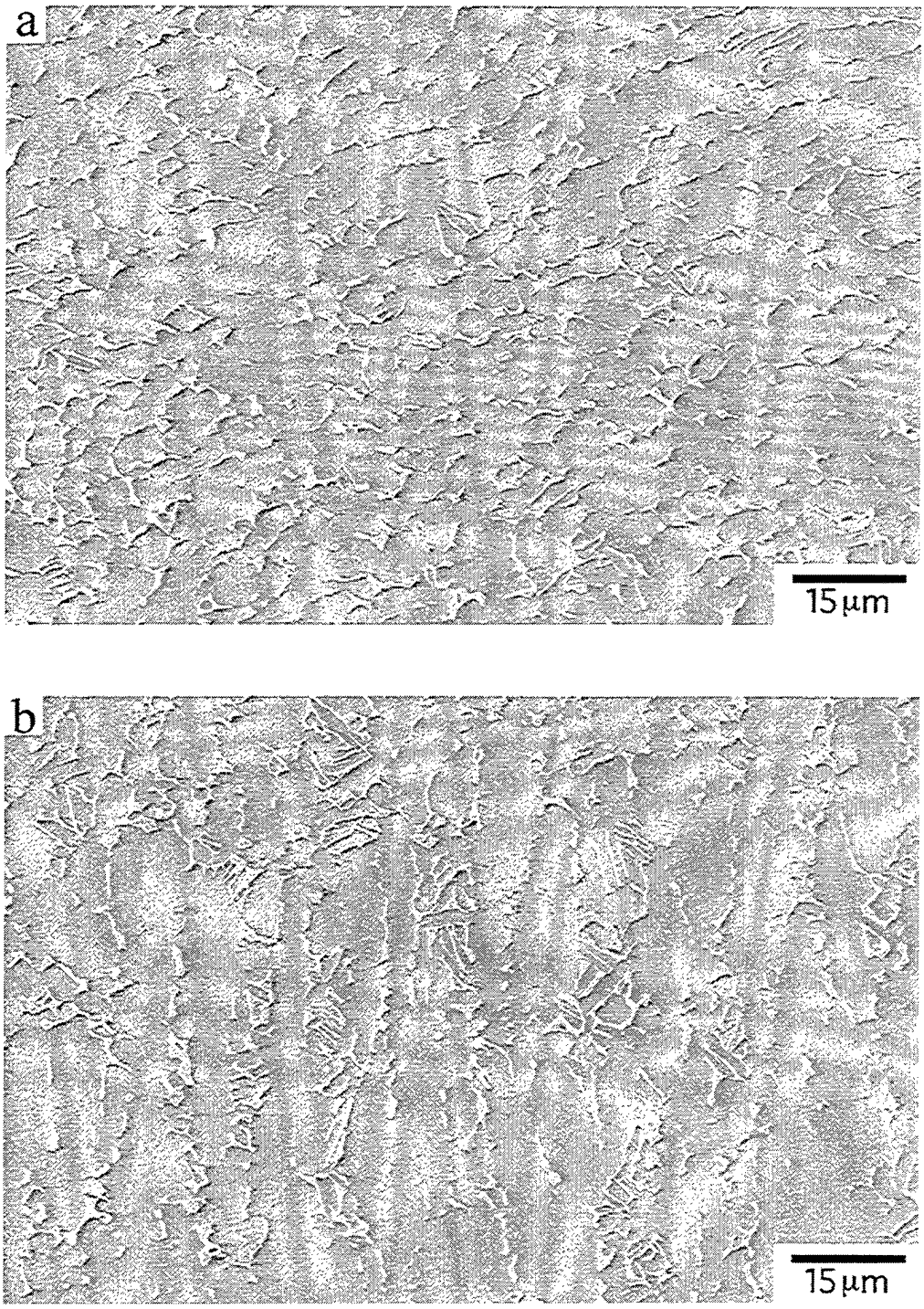

Figure 3-1. Ti-6Al-4V microstructure: a) transverse, b) longitudinal

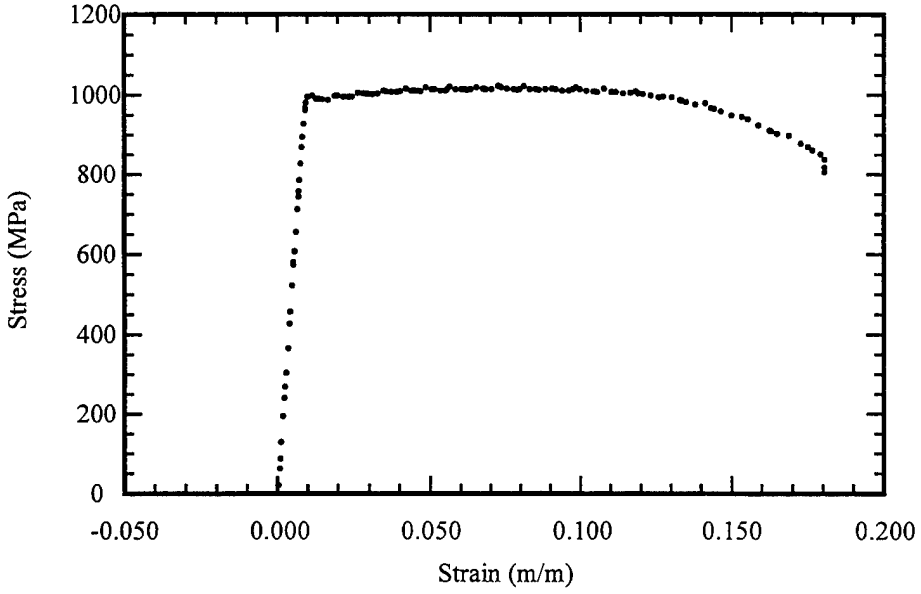

Figure 3-2. Engineering Stress Strain Curve for Ti-6Al-4V

3.2 HCF Tests

HCF testing was performed in the Materials Behavior Branch of the Materials Directorate, which is contained within the U. S. Air Force's Wright Laboratory located at Wright-Patterson AFB, OH. Tests were performed at this location due to the availability of high frequency test frames.

Test System

Two different test systems were used to complete the HCF testing for this project. The first, which was used for all 70 and 400 Hz testing, consisted of a shaker

system and is schematically shown in Figure 3-3. It consisted of a pneumatic actuator and a C10 electromagnetic shaker which were responsible for the "static" load and the super-imposed high frequency load, respectively. A steel crosshead was used to hold the 20 kN load cell. A flowchart depicting the main characteristics of the system is shown in Figure 3-4. Additional figures of the test system can be found in Appendix C.

The system was aligned with a straight, stainless steel specimen. The specimen was loaded into the machine, and then the woods metal which holds the load cell in alignment was melted. This allows the load cell to move freely. After the load cell has reached its equilibrium position, the woods metal was allowed to cool and the system was once again rigid. Strain gages were then attached to one of the specimens which were used in this study. The strain gages were attached 90° apart and load was slowly applied to the specimen. This was useful for a number of reasons: it provided a way to see if strain readings were the same on all sides of the specimen, determine if any bending was present, and calibrate between actual loads and load cell readings. While the load was still being applied, a frequency scan was performed to provide a calibration curve. For the tests in this study, the calibration factor was 1.0 at 70 Hz for all dynamic amplitudes, indicating that the load cell was reading the actual stresses in the specimens. At 400 Hz, some error was detected in load cell readings as a function of dynamic load. Because of this error, a calibration factor of 1.025 was used in the tests performed at 400 Hz to

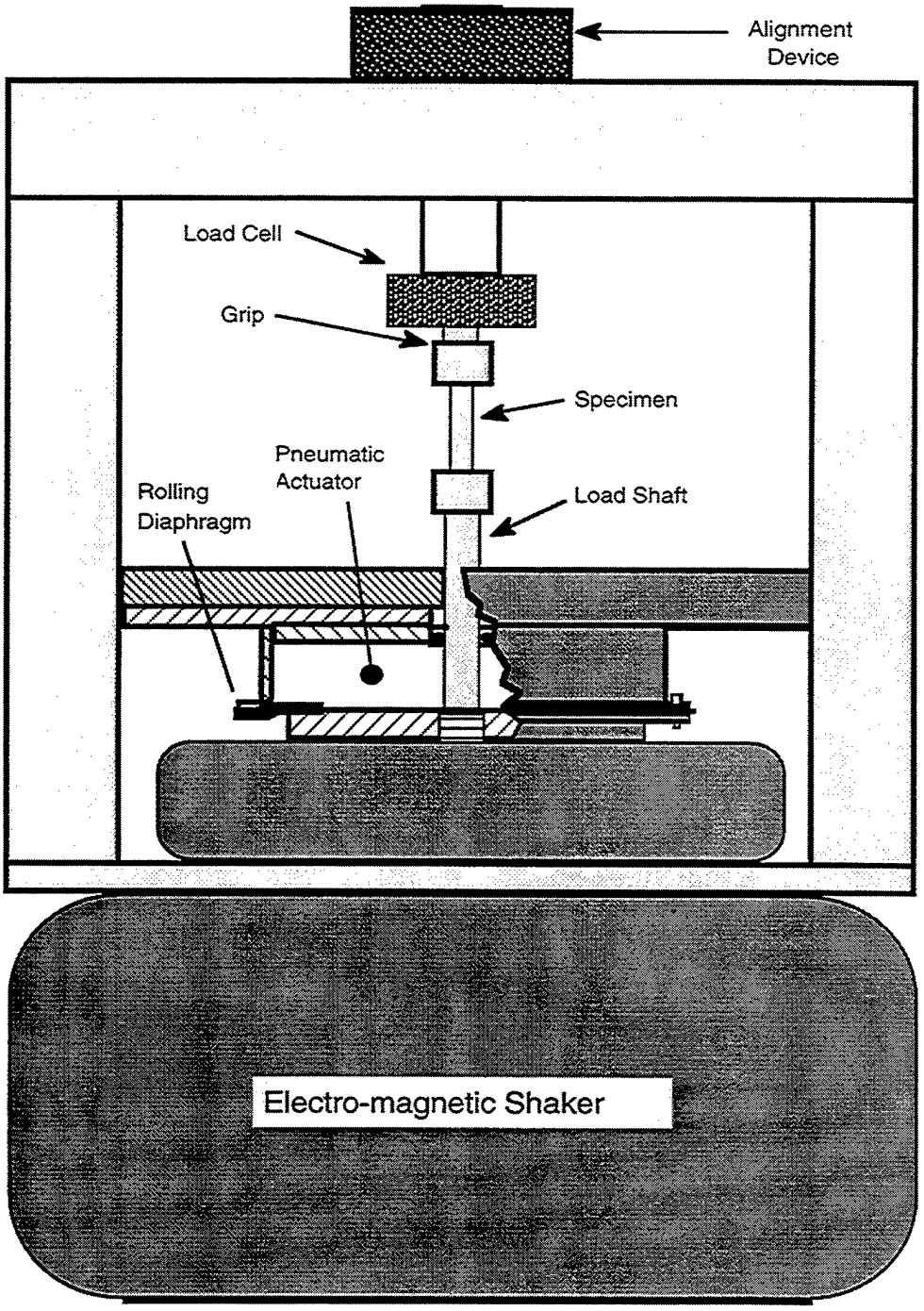

Figure 3-3. Schematic Diagram of Electromagnetic Shaker System

(not to scale)

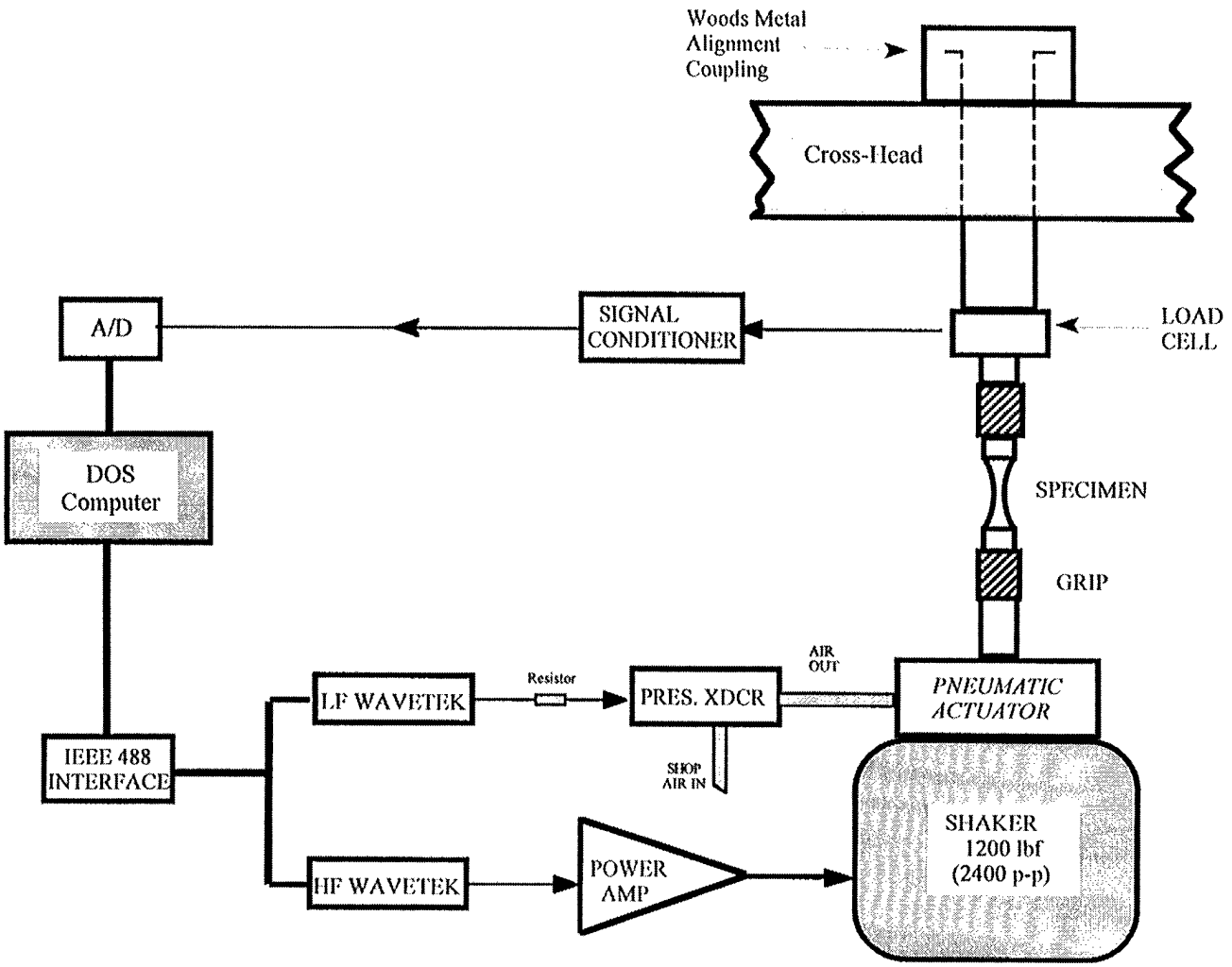

Figure 3-4. C10 HCF Test System Component Schematic

determine the actual stresses present during the experiments. No significant bending was found in the configuration.

In addition to the standard configuration, tests performed at 70 Hz were compared with tests which had been performed at an earlier date on a standard MTS load frame on the same material [32]. As can be seen in Figure 3-5, excellent agreement was shown between the data. This provided secondary validation of the accuracy of the test system.

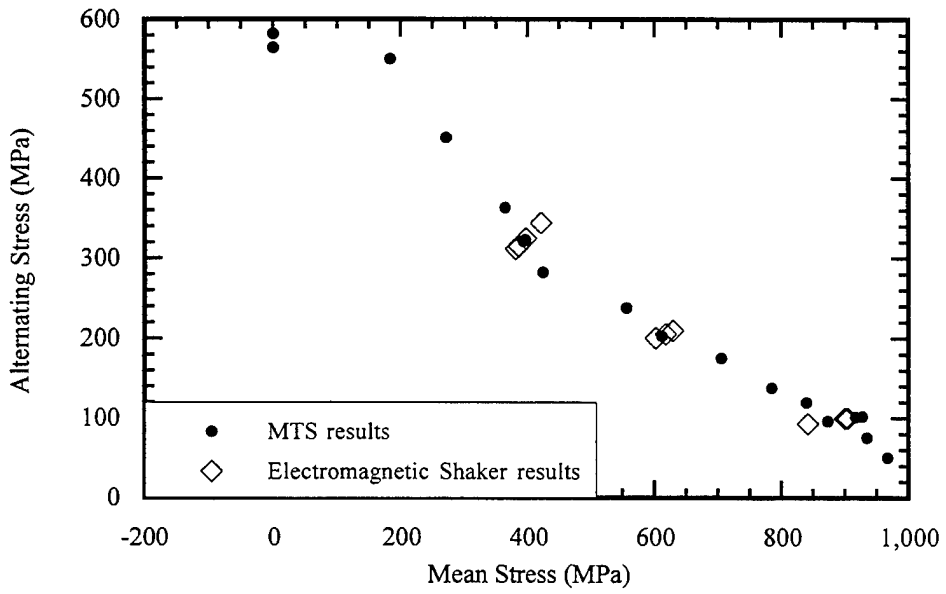

Figure 3-5. Comparison of Results between MTS System and Electromagnetic Shaker (70 Hz)

Data acquisition was performed using the Materials Analysis and Test Environment (MATE) system software [33] on a 286 IBM compatible computer. The MATE software is capable of controlling various types of mechanical testing and storing a wide range of test information. Data were taken at prescribed intervals during the testing, at which point the dynamic load would return to zero. This allowed data to be taken at the mean load each time, making future comparison of data easier. The data which were collected included cycle count, elapsed time, mean load, maximum load, and stress ratio. In addition, the program kept track of the fluctuation of the maximum load during the test. The error in maximum load was generally no greater than 1 percent during a single test.

A LaserMike laser micrometer was used during a portion of the HCF tests to determine the elongation of the specimen during testing. The laser micrometer measured the distance between the upper and lower grips. This allowed the elongation of the specimen to be determined throughout the test. The measurements were taken each time the MATE software took data. The laser micrometer took 128 measurements, which required just over one second, and then sent the average measurement to the MATE software to be recorded.

The second test system was used for all 1800 Hz testing. It was a prototype design (patent pending) developed by The University of Dayton Research Institute in

conjunction with the Materials Behavior Branch at Wright-Patterson AFB. It utilizes a magnetostrictive actuator to active loads at very high frequencies. The details of the system cannot be described here due to its proprietary nature.

Calibration for this test system was performed in a manner similar to the shaker system.

Specimen Design

Buttonhead specimens (Figure 3-6) were used with the shaker system, and were machined and polished by BITEC CNC Production Machining, Dayton, OH. The specimens were machined using a low-stress-grind technique, and then polished to produce a 15 micron surface finish. Original specimen designs consisted of a diameter of 9.53 mm. at the widest point in the grips, and a gage section diameter of 4.76 mm. In addition, a section of the gripping area is machined down to a diameter of 7.14 mm to allow collets to grip the specimen. Two changes were eventually made to the specimens due to initial failures in the grips. The gage diameter was decreased to 3.81 mm, and a larger radius of curvature was used at the buttonheads. This was sufficient to guarantee that the largest stresses would occur within the gage section and prevent further specimens from breaking in the grips.

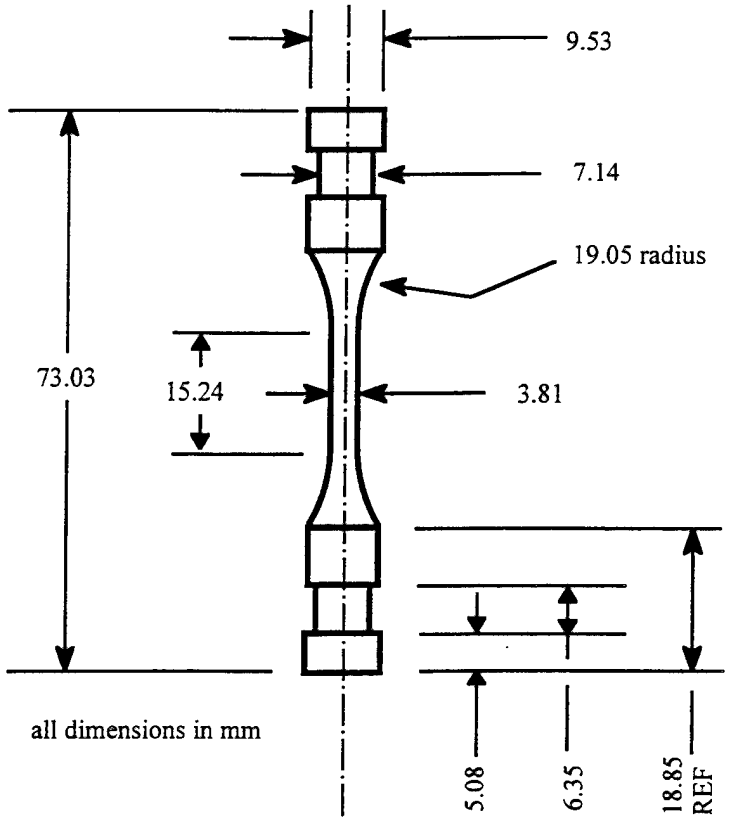

Figure 3-6. Buttonhead Specimen Used in HCF Testing

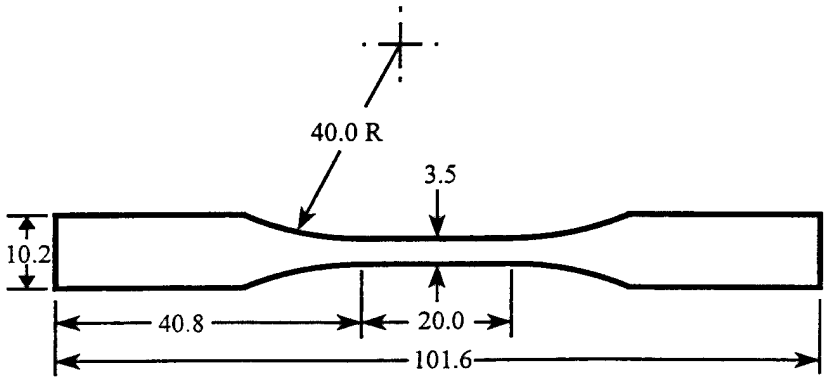

Figure 3-7. Creep Specimen

Similar specimens were used for the 1800 Hz testing, with just slight modifications in design to accommodate the different gripping system.

Test Matrix

The test matrix is shown in Table 3.3, and consists of three tests at each frequency and stress ratio. Additional tests were run as time allowed. Due to the limited load capacity of the high frequency test system, no 1800 Hz tests were run at a stress ratio of 0.1.

Table 3-3. Test Matrix

Stress Ratio	Frequency (Hz)	Number of Tests Performed
0.1	70	3
	400	3
	1800	0
0.5	70	3
	400	3
	1800	3
0.8	70	3
	400	3
	1800	2

Tests to determine the fatigue limit stress were run in a manner developed in previous work at the Materials Lab [32]. For the purposes of the investigation, the fatigue limit was defined as the stress below which fatigue failure does not occur in 10^7 cycles. The test method consisted of cycling specimens to 10^7 fatigue cycles at a stress level which is below the expected fatigue limit. If failure does not occur within 10^7 cycles, the maximum stress was increased by a small amount, 20-25 MPa, and the cycling is resumed at the same stress ratio for 10^7 cycles. This procedure is repeated until failure occurs during a loading block. The small increase in maximum stress is used to decrease the error in determining the effective fatigue limit. The number of cycles to determine the fatigue strength of the material was chosen as 10^7 because that is a number commonly used in the design of rotating engine components.

The maximum stress of the final and prior loading block are used to determine the effective stress which would cause failure in 10^7 cycles. This is done by using a linear interpolation of the form:

$$\sigma_o = \sigma_{pr} + \frac{N_f}{10^7}\left(\sigma_f - \sigma_{pr}\right) \tag{3.1}$$

where σ_o is the maximum stress corresponding to 10^7 cycles, σ_f is the maximum stress during the final loading block, σ_{pr} is the maximum stress during the last completed block, and N_f is the number of cycles to failure within the final block. This method of

determining the fatigue limit at a particular number of cycles has been tested and validated to give very consistent results with standard procedures using multiple specimens [32].

3.3 Creep Tests

Static creep tests were also performed in the Materials Behavior Branch of the Materials Directorate. Tests were completed at stresses ranging from 850 MPa to 950 MPa. The tests were run for 100 hours, unless fracture occurred. This time was chosen to approximate the duration of the HCF tests.

Test System

Creep tests were performed using a standard horizontal MTS test frame. A MTS clip gage was attached to the specimen to measure the strain. Data were collected using the MATE software [33].

Specimens

Flat, rectangular dogbone specimens were used for the creep tests. The specimens were 101.6 mm long, with a gage section width of 3.75 mm and a thickness of 1.0 mm, as shown in Figure 3-7.

CHAPTER IV

RESULTS AND DISCUSSION

4.1 Frequency Effects

Maximum stresses were found which gave fatigue lives of 10^7 cycles for stress ratios of 0.1, 0.5, and 0.8 at frequencies of 70 and 400 Hz. Tests at stress ratios of 0.5 and 0.8 were also performed at 1800 Hz. The maximum are listed in Table 4-1. The values listed are averages of all tests performed at each frequency and stress ratio. A complete list of results can be found in Appendix A. The results can also be seen in Figure 4-1, which shows the averages plotted on a Goodman Diagram as a function of mean stress and stress amplitude. Very little scatter was apparent during the testing at frequencies of 70 and 400 Hz, although there was appreciable scatter at 1800 Hz.

Also listed in the Table 4-1 are the average strain rates for each test. The rates listed are elastic strain rates, and were calculated by dividing the stress range by the Young's Modulus and multiplying by the frequency. The final column lists the strain rates normalized with respect to the strain rate at 70 Hz with a stress ratio of 0.8. This was done to facilitate comparison of the relative strain rates at each stress ratio and

Table 4-1. Results of HCF Testing

Stress Ratio	Frequency (Hz)	Maximum Stress (MPa)	Strain Rate (m/m/s)	Normalized Strain Rate (wrt 70 Hz)
0.1	70	720	0.42	3.31
	400	773	2.55	20.30
0.5	70	821	0.26	2.10
	400	876	1.61	12.77
	1800	1025	8.47	67.26
0.8	70	980	0.13	1
	400	982	0.72	5.73
	1800	1069	3.53	28.04

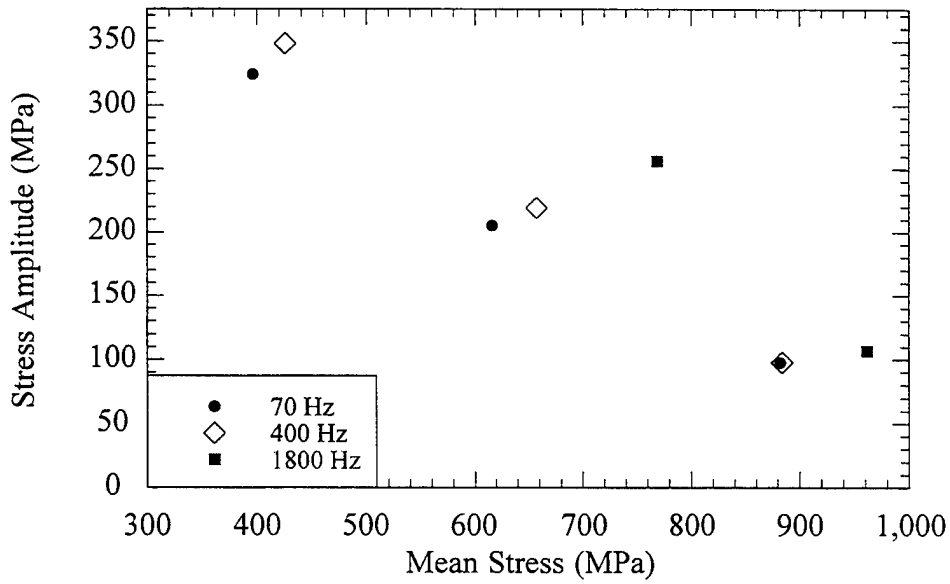

Figure 4-1. 10^7 Cycle Fatigue Strengths at Frequencies of 70, 400, and 1800 Hz.

(Stress Ratios of 0.1, 0.5, 0.8)

frequency. In general, the strain rates at 400 Hz were approximately six times those at 70 Hz, and the 1800 Hz rates were thirty times the 70 Hz rates. Testing at stress ratios of 0.1 produced strain rates approximately three to four times those at 0.8, while those at stress ratios of 0.5 were over twice as high as the 0.8 rates. These relatively small differences (less than an order of magnitude) were observed to be sufficient to produce very distinct differences in the fatigue strengths.

The results indicate that there is a significant frequency effect in Ti-6Al-4V, especially at low stress ratios. The higher the frequency, the higher is the stress which will cause failure in 10^7 cycles. This is an important factor to consider, especially when most testing is done in this regime of the Goodman diagram. The mechanisms which are responsible for this phenomenon are presently unknown, but there are a few possibilities, as discussed next.

Strain Rate

One factor which influences the observed frequency dependence of Ti-6Al-4V is the material strain rate dependence of plastic flow. Many materials and alloys, including Ti-6Al-4V, have shown evidence of a strain rate effect in constant strain rate testing. Nicholas [34] showed that for a constant value of strain, the flow stress increased with increasing strain rate. Strain rate dependence was small at rates similar to those in this experiment, but the effect was magnified at higher rates. These results are consistent with

the results of this investigation, which showed a small increase in Goodman stress when the frequency was increased from 70 to 400 Hz, and a larger increase as the stress is further increased to 1800 Hz. A common interpretation of the strain rate effect is that as the frequency of loading is increased, dislocations have less time to overcome obstacles via thermal activation, thereby reducing the amount of plastic strain accumulated. This could become very important if the material is susceptible to cyclic ratchetting. Higher frequencies will require higher loads to produce the same strain range. In addition, this effect would be amplified at lower stress ratios, where the dynamic amplitude is greatest. Since fatigue is a plasticity-induced phenomenon, this could explain the increased fatigue strengths at higher frequencies. The possible contributions by cyclic ratchetting to the strain accumulation will be discussed in more detail in a later section.

Another possibility involving the strain rate is a dependency on the crystal structure of the material. As was mentioned in Chapter II, lattice structure has been linked to a frequency effect. Roth *et al.* [10] explained this effect in terms of the slip systems of the material, which are dependent on the crystal structure. Many of the slip systems in FCC metals remain active at high frequencies. In contrast, fewer slip systems remain active in BCC materials at high frequencies. This may be a result of the relative numbers of primary slip systems available in each structure. FCC materials contain twelve primary slip systems, whereas BCC materials only contain five primary in addition to its 48 seconday slip systems. One might extrapolate these findings to HCP

structures, which contain only three primary slip systems. At low temperatures, HCP structures are limited to basal slip, thereby reducing the amount of plastic deformation which can occur. Since Ti-6Al-4V contains predominately HCP α phase, with the balance being the BCC β phase, a significant frequency effect might be expected [10].

Environment

Another contributing factor to the frequency effect could be environmental effects. Peters *et al.* [12] have shown large decreases in the fatigue strength of Ti-6Al-4V in air when compared with that in a vacuum. In addition, the fatigue life in air was much closer to lives observed in 3.5 percent NaCl solution than to those measured in a vacuum test. This damage has generally been explained as a result of hydrogen embrittlement. Demulsant and Mendez [11] have discussed the possible effect of hydrogen embrittlement on fatigue crack initiation and propagation in titanium alloys.

If the laboratory air does have an impact on the fatigue life, lower frequencies should exhibit shorter lives due to the increased amount of testing time required for similar numbers of cycles. Tests performed at these lower frequencies would allow more time to accumulate environment assisted damage. This is also consistent with the results of this investigation.

Temperature Effects

An increase in temperature occurring within the specimen is a concern when testing at high frequencies. This is especially true at low stress ratios, where the dynamic amplitudes are the greatest. However, internal heating would produce more damage within the material, thereby reducing the fatigue life. This would imply that higher frequency testing would result in lower fatigue strengths, which is not the case. It is therefore believed that temperature rise within the specimen is not a significant contributing factor at the frequencies considered here, and any effect it may have is secondary.

Creep

Time-dependent creep is not generally considered to be important in HCF, but may play an important role at high stress ratios, where a portion of each cycle is spent at stresses near or above the static yield stress of the material. Ti-6Al-4V is widely known to experience room temperature creep at stresses lower than those experienced in this investigation. In addition, cyclic creep rates in some materials have been shown to exceed static rates. As the frequency is increased, less time is spent at each loading block, thereby reducing the effect of creep. This suggests that higher frequencies would result in increased fatigue strength. The results at the high mean stresses are conflicting in this study. The specimens tested at 1800 Hz showed a much higher fatigue strength than

those tested at 70 and 400 Hz, although the difference was less than it had been at a stress ratio of 0.5. The fatigue strengths at the lower frequencies were practically identical, differing by only 0.2 percent. These results may indicate competing mechanisms in the material. The creep effect will be discussed in more detail in a later section.

4.2 Mean Stress Effects

The effect of mean stress in HCF applications has received a lot of attention for years, and many design methodologies have been suggested. Perhaps the most popular of these is the Modified Goodman Diagram, a plot of mean stress vs. stress amplitude for a prescribed number of cycles. Modified Goodman Diagrams can be extremely useful in determining the allowable stress amplitude for different values of mean stress. Problems can arise at high mean stresses, however, due to the large amounts of scatter in this region. In addition, these diagrams give the impression that fatigue due to the stress amplitude is the crucial factor in determining a components life. This may not always be the case. At high stress ratios, the mean stress can be very near the static yield stress, and the maximum stress may even exceed the static ultimate strength of the material. In addition, stress amplitudes are low. The effects of these high stress ratios is discussed in the following sections.

Failure Mechanisms

The fracture surface at the lower stress ratios, as seen in Figure 4-2, showed evidence of fatigue crack growth followed by ductile tearing and shear lip formation near the surface. The fatigue crack growth region was characterized by cleavage fracture and exhibited large facets. In addition, striations could be seen on the surface of individual facets at very high magnifications. Examination of these SEM fractography pictures for one specimen, R = 0.5, showed the crack growth region to be approximately 18% of the fracture surface. The nominal maximum stress at fracture was 820 MPa, which corresponds to an actual maximum stress of 1000 MPa when the reduced area is taken into account. This stress is close to the static ultimate stress of the material, and could explain the subsequent ductile tearing to failure following the crack growth. A second specimen, R = 0.7 [32], showed the crack growth region to be an almost identical percentage of the fracture area, 17%. These are rough estimates since the transition between these two regions is not clearly defined.

Failure in HCF is normally associated with this type of fatigue crack growth and subsequent failure. This is not necessarily the case, however, at high stress ratios (R > 0.75). In this regime, maximum stresses can easily exceed the static yield stress of the material, with mean stresses being larger than 0.9 times the yield stress. Sustained cycling at such high stresses over a long period of time can lead to excessive strain accumulation

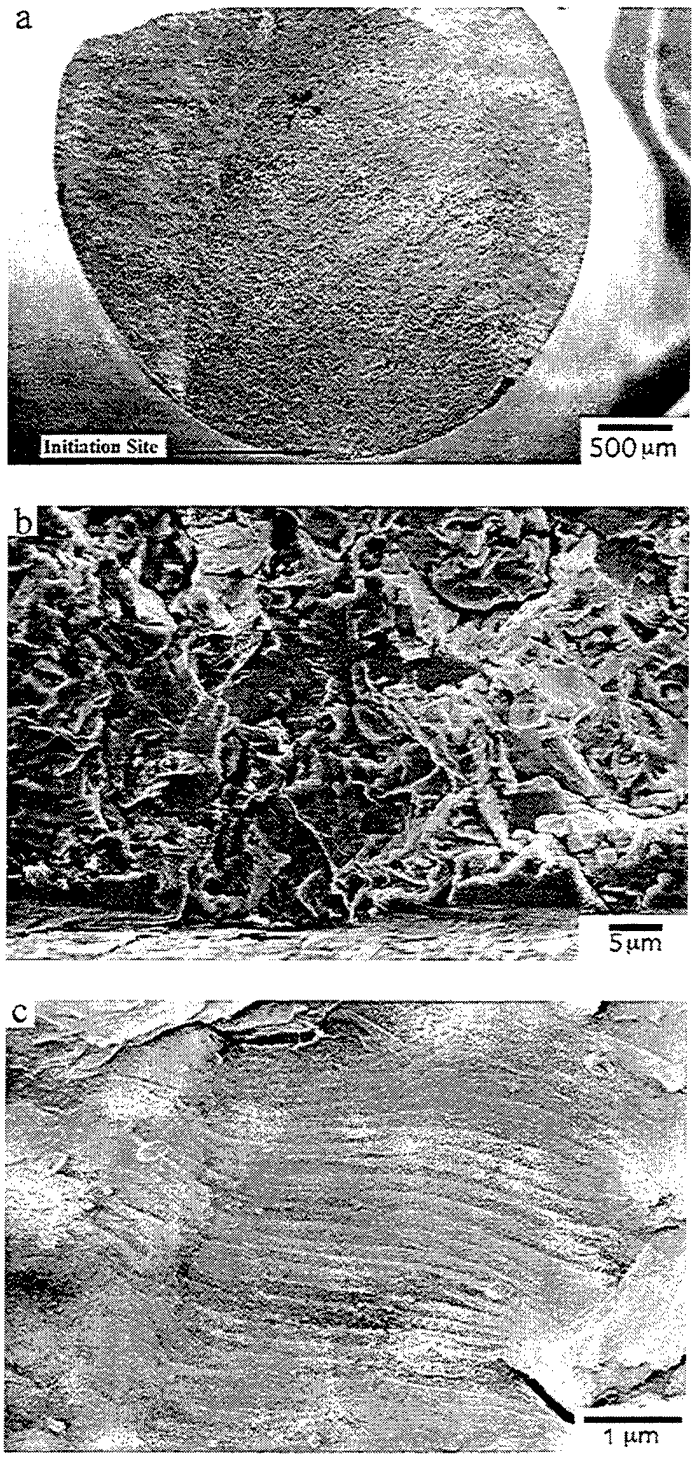

Figure 4-2. Fracture surface of HCF specimen, R = 0.5: a) macroscopic view, b) initiation site, c) striations near initiation site.

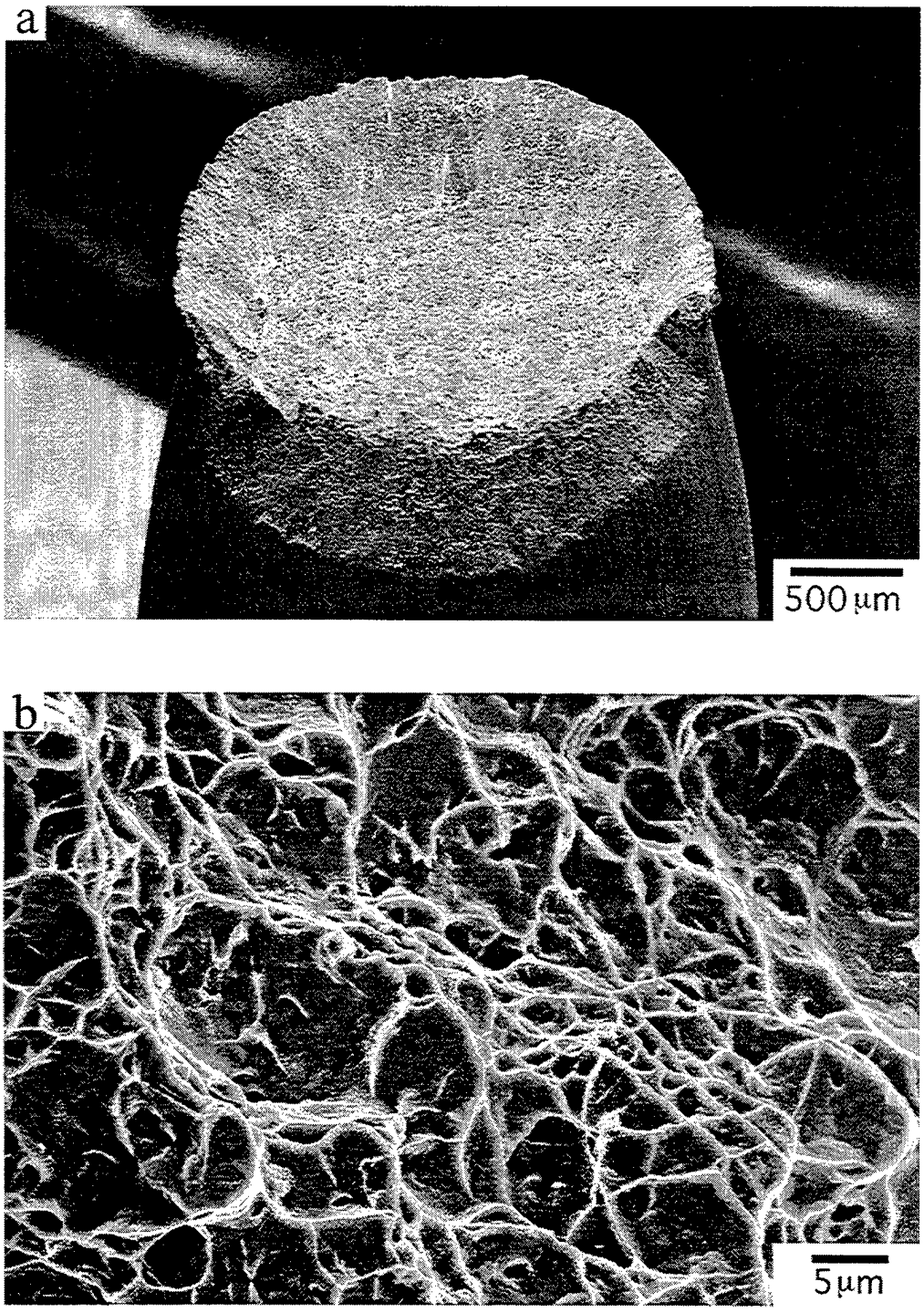

Figure 4-3. Fracture surface of HCF specimen, R = 0.8

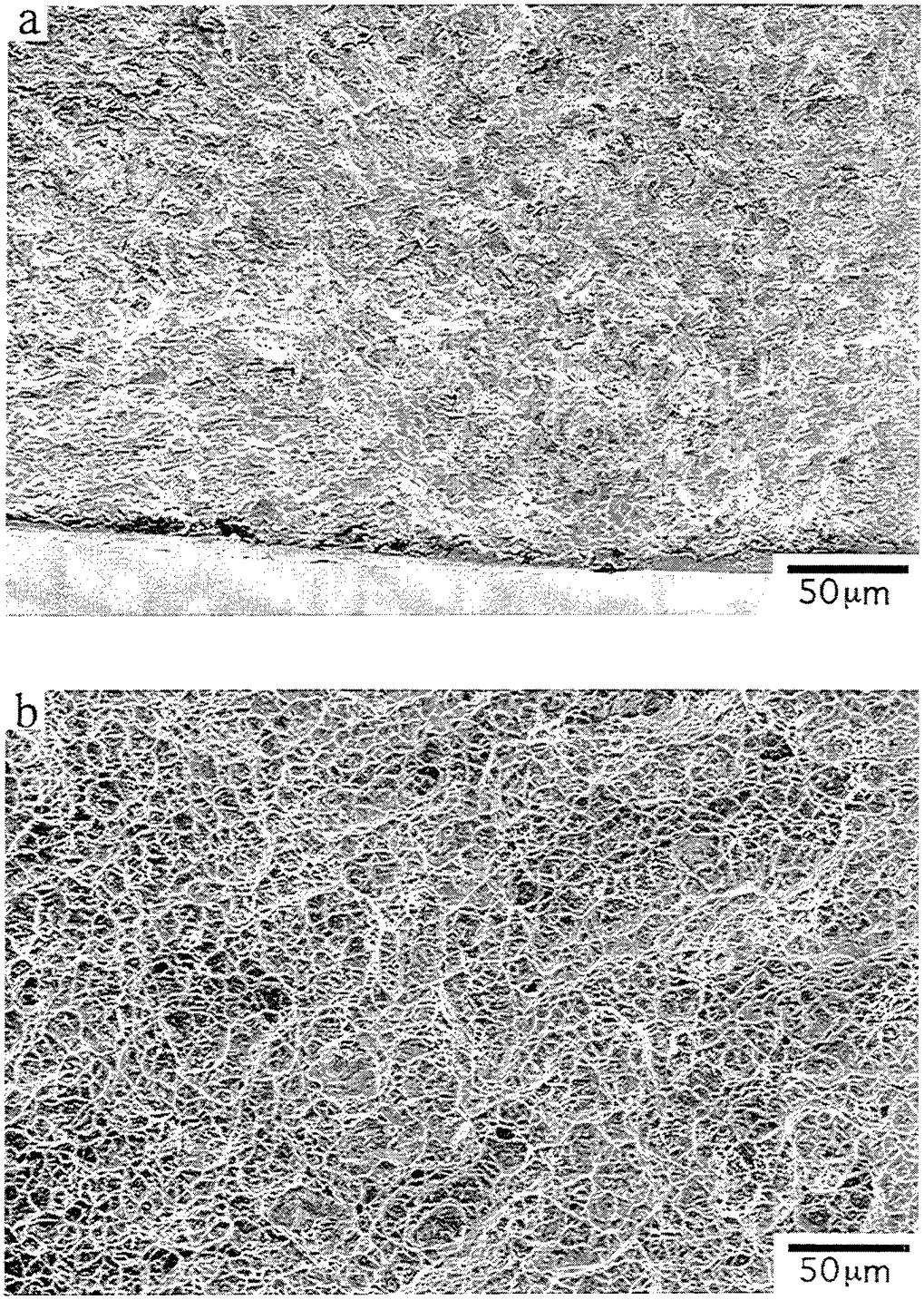

Figure 4-4. Comparison of Fracture Surface Under Varying Conditions: 70 Hz HCF testing at a) R = 0.7, b) R = 0.75

which may result in a ductile failure mechanism, as evidenced by the necking which occurred at a stress ratio of 0.8.

Detailed examination of the fracture surface makes this effect very apparent. Figures 4-2 and 4-3 show the fracture surfaces at two stress ratios, R = 0.5 and R = 0.8 at two magnifications. It is evident that the fracture mode is quite different. In addition, samples tested in a separate study [32] show that the transition between these modes is very abrupt: In this case it occurs between R=0.7 and 0.75. Figure 4-4 shows the fracture surfaces at these two stress ratios.

An empirical explanation of this phenomenon can be seen from Figure 4-5. This plot shows the maximum and minimum stresses required to cause failure in 10^7 cycles plotted as a function of mean stress. The data were taken from the previously mentioned study, and covers stress ratios from -1.0 to 0.9. A line has been drawn horizontally to correspond to a maximum stress of 875 MPa. This particular value corresponds to the stress at which strain accumulation due to creep could be expected based on the creep tests performed in this study. At this maximum stress, the corresponding minimum stress can be estimated from the Figure as 530 MPa. These stresses correspond to a stress ratio of 0.6, and can be used to estimate the point at which plastic strain accumulation due to cyclic creep may begin to contribute to the failure process. This contribution should increase as the maximum stress increases and a larger portion of each cycle experiences such stresses. As was mentioned previously, the point where these

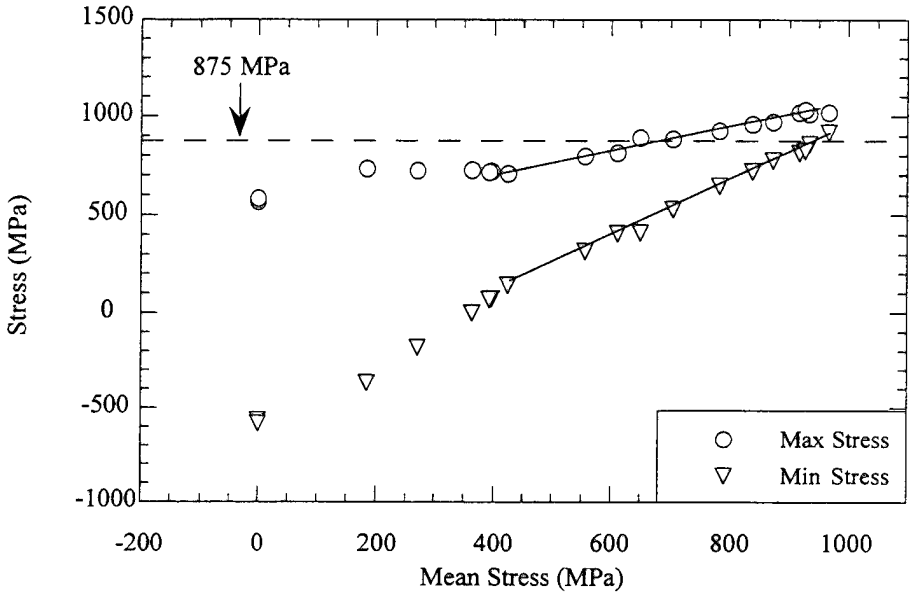

Figure 4-5. Plot of Maximum and Minimum Stress Versus Mean Stress at 70 Hz

stresses have been shown to be sufficient enough to cause ductile fracture occurs at stress ratios larger than 0.7. While this example is entirely without a theoretical basis, it can nevertheless be used to appreciate the effect of high mean stresses on fatigue.

Frequency does not seem to play a major role in the fracture mode based on the fractography of the fracture surfaces. No apparent differences are seen in the fracture surfaces at a stress ratio of 0.8 for different frequencies. This can be seen in Figure 4-6. In addition, these fracture surfaces appear identical to the fracture surface of a creep specimen. These results indicate that a similar mechanism is responsible for the bulk

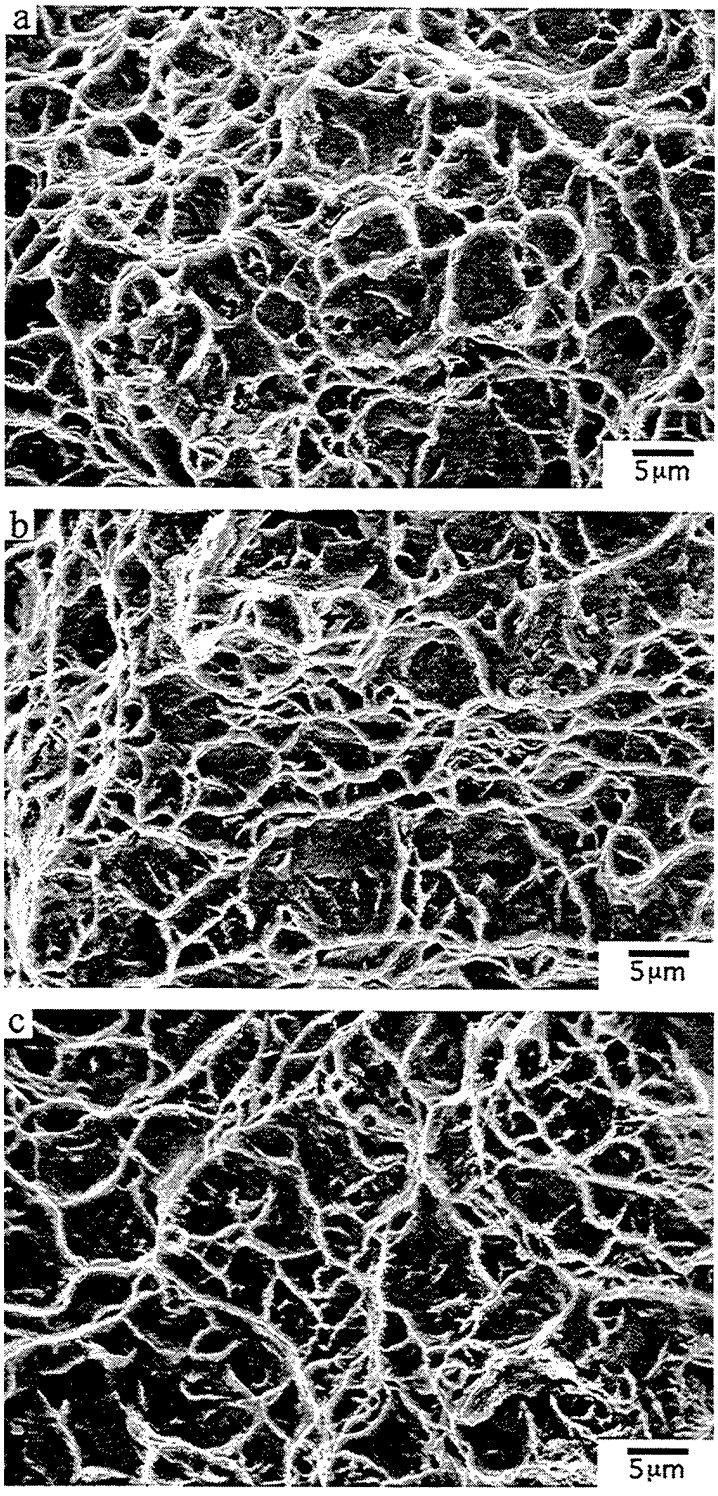

Figure 4-6. Comparison of Fracture Surface Under Varying Conditions: a) 70 Hz, b) 400 Hz, c) Static Creep, 943 MPa

damage and subsequent failure due to void nucleation and growth. Similarly, the fracture surfaces at the three frequencies for a stress ratio of 0.5 are also identical. One may surmise that the actual transition between failure modes may change at different frequencies, but additional testing would be required to prove any such hypothesis.

4.3 Cyclic Strain Accumulation

In order to determine the amount of strain accumulation occurring during HCF, a laser micrometer was used to measure the elongation of the specimen during the fatigue testing. Figure 4-7 shows a typical plot of elongation as a function of cycles at a stress ratio of 0.8. At stress ratios of 0.5 and 0.1, no progressive change in displacement could be measured within the resolution of the laser micrometer.

Cyclic Creep

Ti-6Al-4V has long been known to exhibit room temperature creep at stresses well below yield. It is therefore likely that the same material will exhibit a similar time dependence during HCF loading. In order to determine the possible effects of time dependent deformation during a fatigue test, room temperature creep tests were performed. The tests were run for 100 hours to approximate the time required to perform the HCF tests. Significant creep was exhibited at stresses greater than 875 MPa, and the

results can be seen in Figures 4-8 - 4-12. Figure 4-13 compares the relative magnitudes of these creeps strains.

Comparisons of this data with the HCF results were made in several ways. A model was developed from the creep data to predict the strain accumulation during the fatigue cycling. This model assumes that cyclic creep will occur due to the same mechanisms as static creep. A detailed analysis of the development of the model and the comparison with the HCF data can be seen in Appendix B.

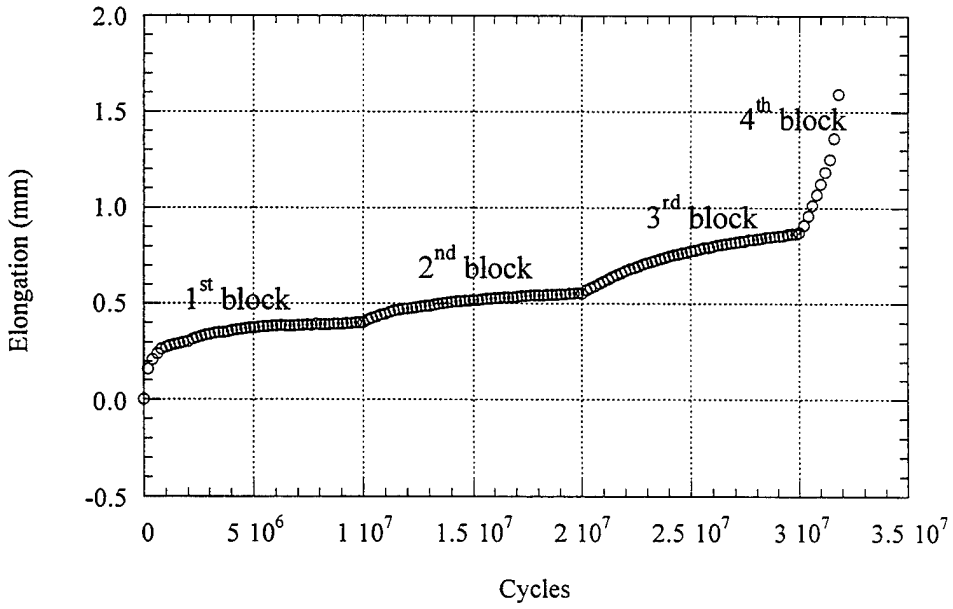

Figure 4-7. Specimen Elongation at Mean Load vs. Cycles

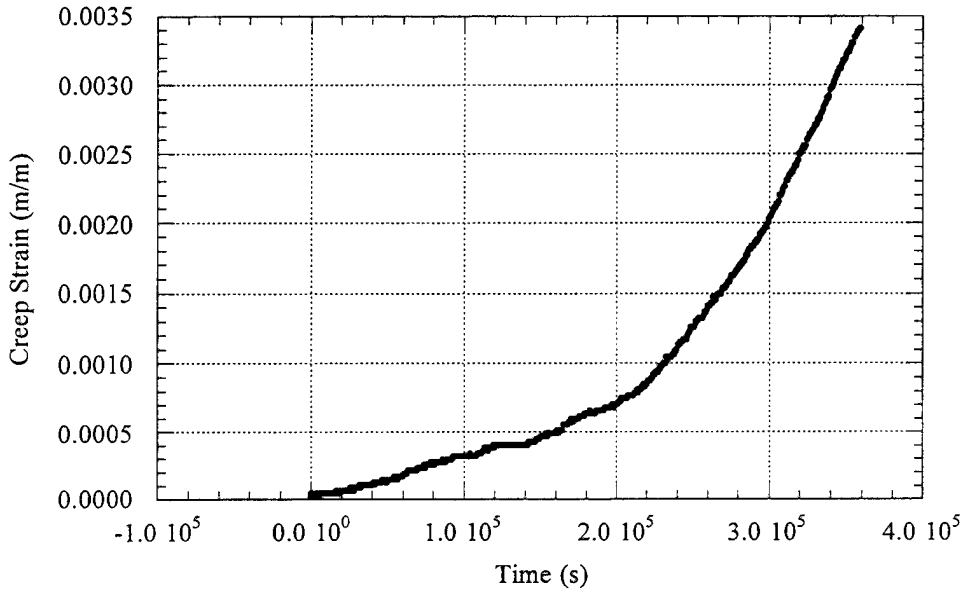

Figure 4-8. Creep Strain vs. Time, 875 MPa

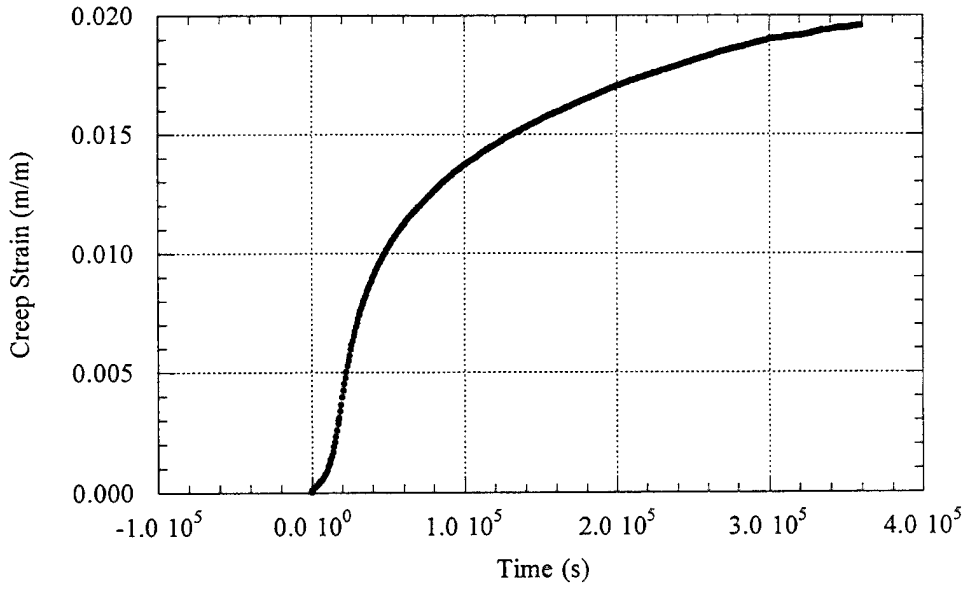

Figure 4-9. Creep Strain vs. Time, 900 MPa

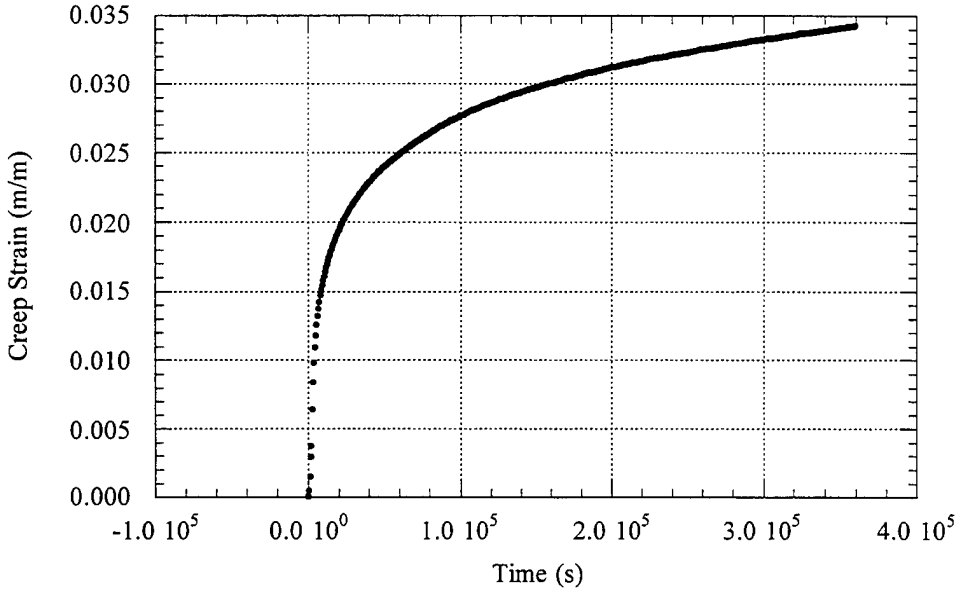

Figure 4-10. Creep Strain vs. Time, 925 MPa

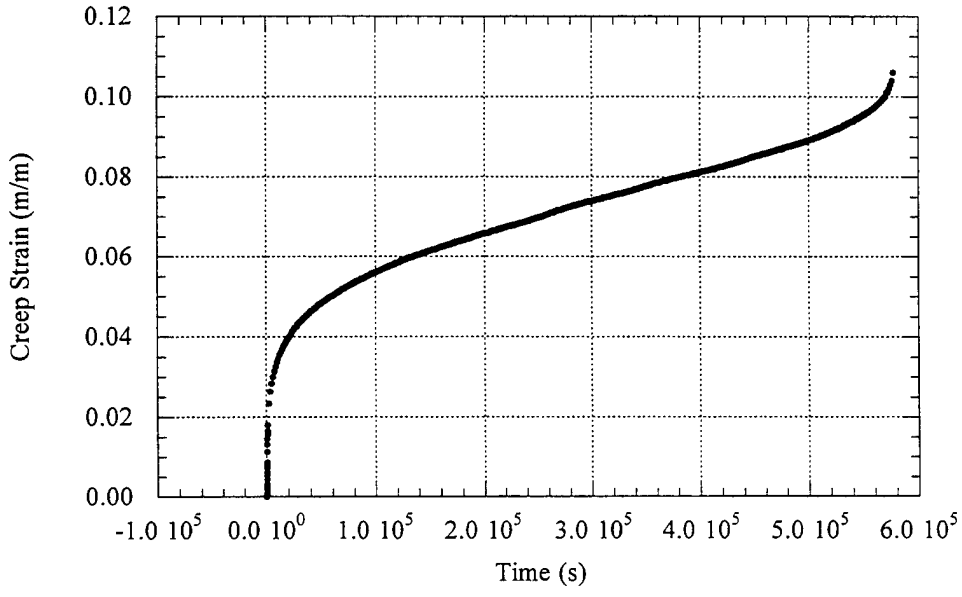

Figure 4-11. Creep Strain vs. Time, 942.5 MPa

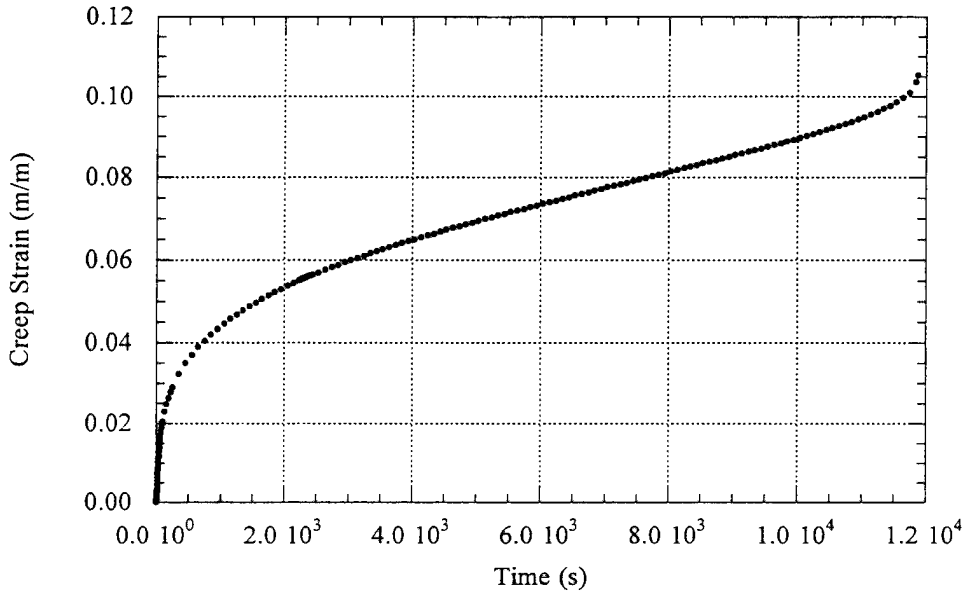

Figure 4-12. Creep Strain vs. Time, 950 MPa

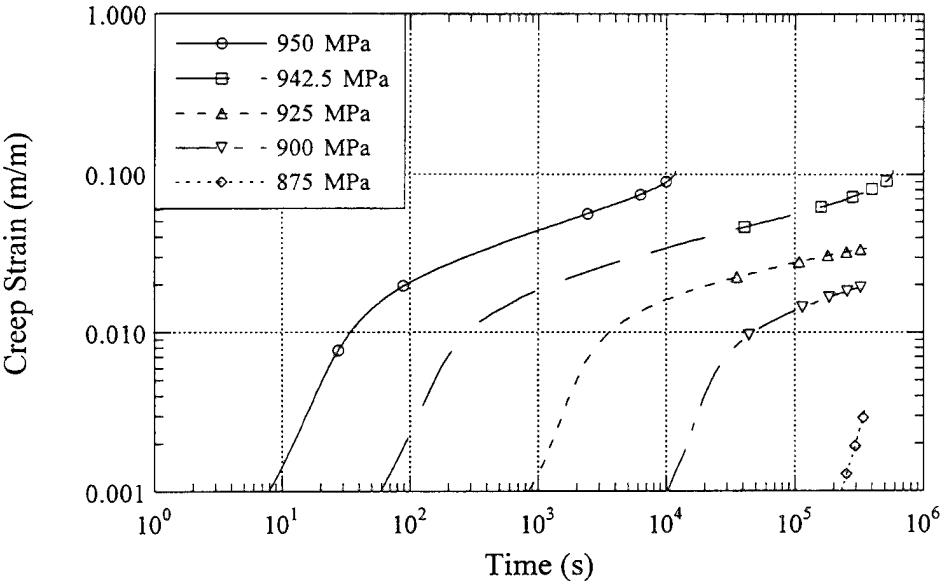

Figure 4-13. Creep Strain vs. Time

As was shown in Figure 4-8 and 4-9, the specimens underwent a softening period in the initial stage of the creep tests. This "inverse creep" was not shown in the literature for room temperature creep of Ti-6Al-4V, but it is a well-known phenomenon [35] in many materials. It is believed that this behavior was not seen in other studies due to the large time intervals between measurements. This investigation concerned itself with creep up to 100 hours, whereas most studies tested to at least 1000 hours. These studies seemed to record data at long intervals due to the length of the tests. This portion of the creep curve seemed to last until approximately 0.3 percent strain, independent of the creep stress.

To simplify the modeling process, this portion of the creep curve is approximated as a linear accumulation of strain. This possible error introduced by this assumption is believed to be negligible due to the small amount of strain which takes place in this region.

The remaining portion of the creep curves were fit with a logarithmic curve. Logarithmic curves have been shown to be in good agreement with creep results for metals at low temperatures [36], and this proved to be the case. The curve fits had correlation coefficients of R2 = 0.99 or higher. The resulting equations were of the form:

$$\varepsilon^{c} = A \log(t) - B \tag{4.1}$$

The resulting curve fit parameters, A and B, from each curve were then plotted as a function of creep stress. A linear curve fit was used to develop an equation for the

logarithmic parameters as a function of stress. The resulting equations for the curve fit parameters were of the form:

$$A = C_1 + C_2 \sigma \qquad B = C_3 + C_4 \sigma \tag{4.2}$$

The final equation for creep strain in terms of time and stress then became:

$$\varepsilon^c = (C_1 + C_2 \sigma) \log(t) - (C_3 + C_4 \sigma) \tag{4.3}$$

In order to model the first portion of the creep curve, the time required to reach 0.3 percent strain at any stress was determined by solving the above equation for t. The linear equation used to model the initial creep behavior then became:

$$\varepsilon^c = \left(\frac{0.003}{t^*}\right) t \tag{4.4}$$

where t* is the time required to reach a creep strain of 0.003 at any specified stress.

In order to model the creep during cyclic loading at R = 0.8, each cycle was divided into a number of discrete steps. In this way, a cycle could be modeled as many small increments of constant stress. This allowed the creep equations to be used to determine the change in strain for each individual step. These changes were then summed to determine the total creep strain accumulation during a cycle.

As was mentioned in the experimental procedure, if a specimen did not break after 10^7 cycles, the maximum stress was increased and cycling was repeated. It was assumed that during the next loading block the initial sharp increase in strain seen in the first loading block would not occur. This was accounted for in the model by resetting the total strain to zero, but letting the time remain at its present value, which varied depending on the frequency. This assumption was verified by visual inspection of the displacement data. Figure 4-14 is typical of the response seen for all specimens tested at R = 0.8. The first loading block always accumulated more strain than the second block, even though it was run at a lower stress.

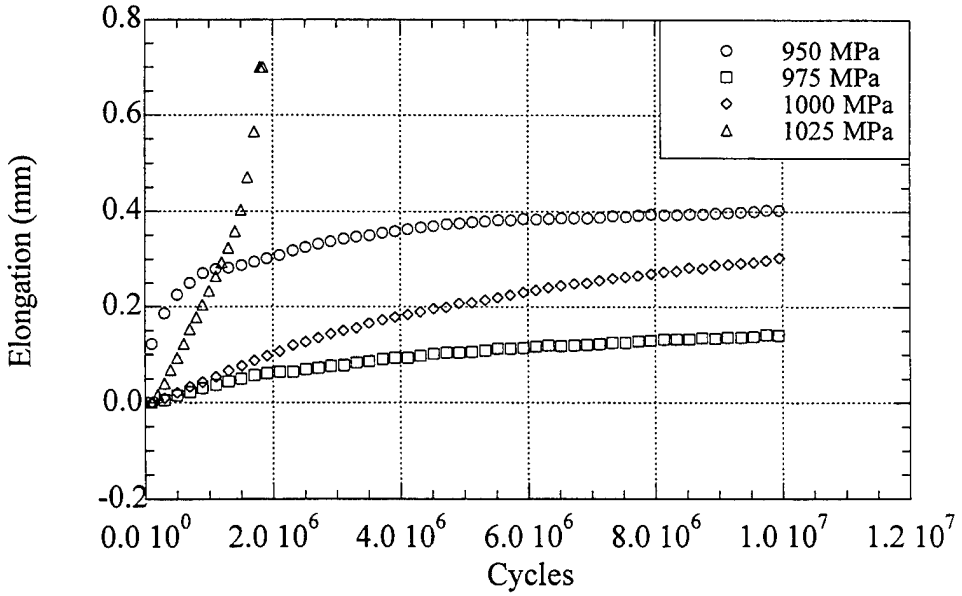

Figure 4-14. Specimen Elongation vs. Cycles at Various Max. Load (R = 0.8, 70 Hz)

The modeling program was written to allow the user to choose the starting cycle and the number of cycles to model. This allowed a small number of cycles to be modeled at various starting positions. The strain rate per cycle was then determined at each position and the total strain accumulated between any two positions was determined by averaging the strain rates and multiplying by the number of cycles. This process was simplified by the use of a spreadsheet, and allowed the total strain accumulated during a loading block to be determined. The intermediate positions at which the strain rates were determined were chosen so that the number of cycles over which interpolation was required grew as the number of total cycles grew. This was done because the fastest strain rates, and the greatest change in strain rates, occur at the beginning of the test, and therefore strain rates must be determined frequently to minimize error. As the strain rates approach steady state, the error introduced by interpolation decreases.

To compare the displacement measurements taken during the HCF tests to the results of the creep model, the displacements were converted into strains using an "effective" gage length. Due to the way in which displacement data were taken, exact calculations of strain were not possible. Instead, values were determined which represented the minimum and maximum, or conservative and non-conservative, possible strains for each test. The minimum possible strain was determined by using the distance between the grips as the effective gage length. Since the stresses experienced by the portion of the specimen outside of the gage section are much lower, it is very unlikely

that this region contributed very much to the elongation. The maximum possible strain was found by using the actual length of the specimen's gage section as the effective gage length. This implied that all measured displacements occurred within the gage section. Since the stresses in this region were much higher than in the rest of the specimen, this assumption should give more reasonable values of strain. It is believed that the actual values of strain lie close to the maximum values calculated. In any case, the true strain should lie between the values determined.

The estimated strains were compared in a number of ways with the results of the creep modeling. A comparison of theoretical strains (from the model) to experimental results is shown in Table 4-2 for each of numerous loading blocks at a stress ratio of 0.8 and frequencies of 70 and 400 Hz. No displacement measurements were taken on the 1800 Hz specimens.

Results of the comparison are consistent for both frequencies. The general shape of the theoretical and actual curves agree for all loading blocks, regardless of frequency. This can be seen in Figures 4-15 - 4-17. During the initial loading block, the theoretical strain closely agrees with the conservative value of strain obtained from experimentation. However, the assumption that the non-conservative calculated strains are the most indicative of the actual strains implies the model severely underestimated the strain accumulation. For subsequent loading blocks, the disparity between the model and the

measurements increases. Time-dependent creep does not seem to be able to account for the total progressive deformation which occurred in these tests.

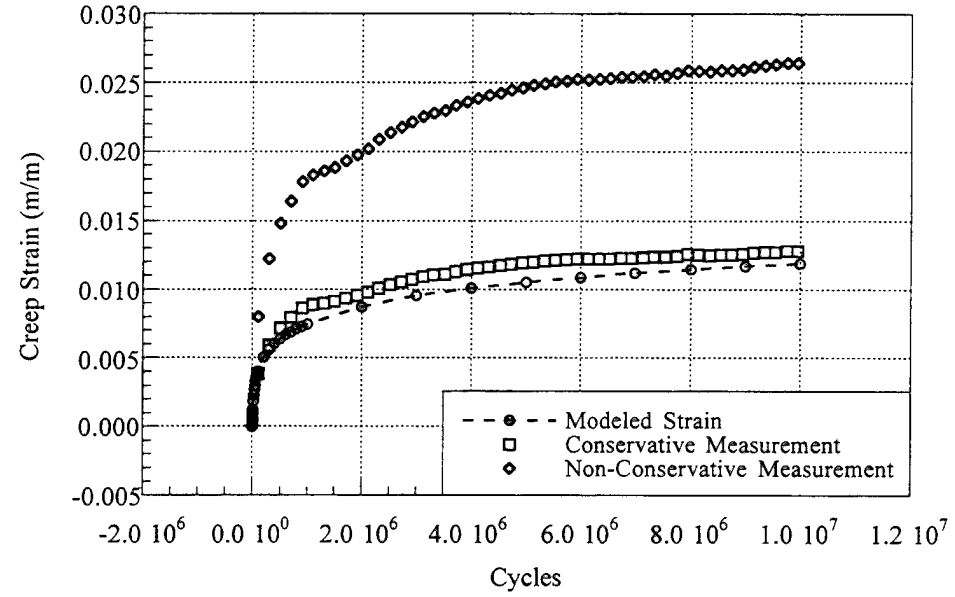

a) 70 Hz

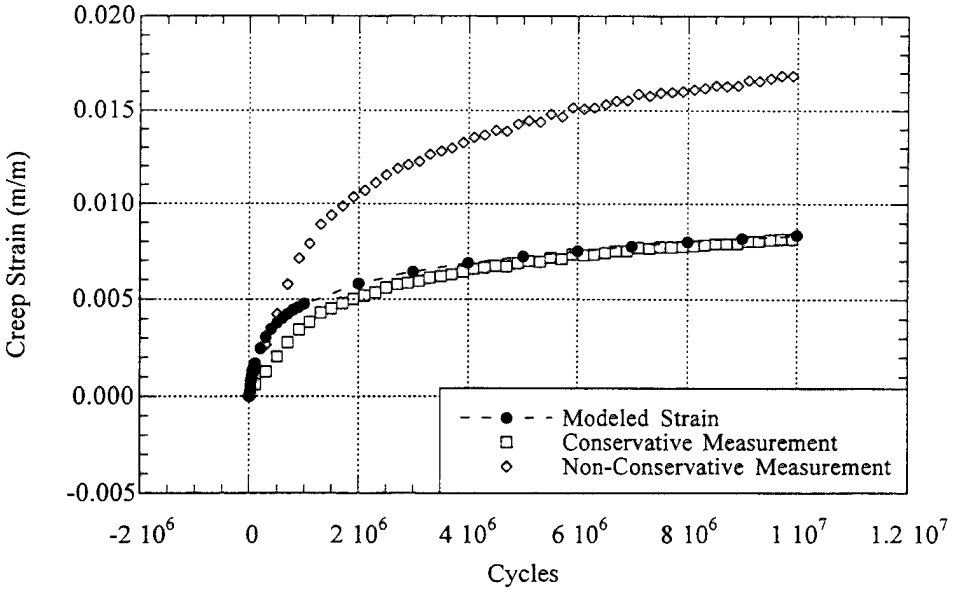

b) 400 Hz

Figure 4-15. Theoretical vs. Experimental Strain

(R = 0.8, 950 MPa - initial loading block)

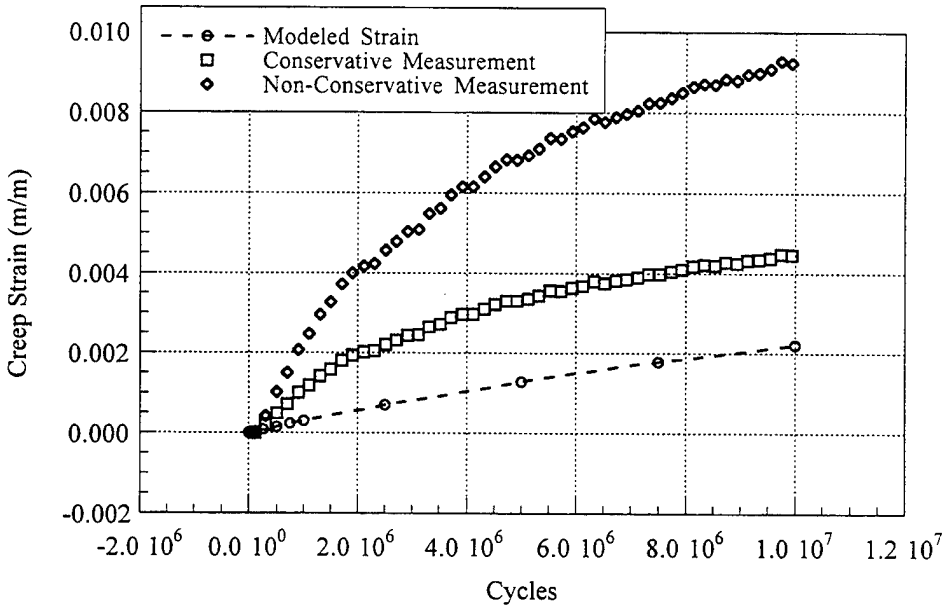

a) 70 Hz

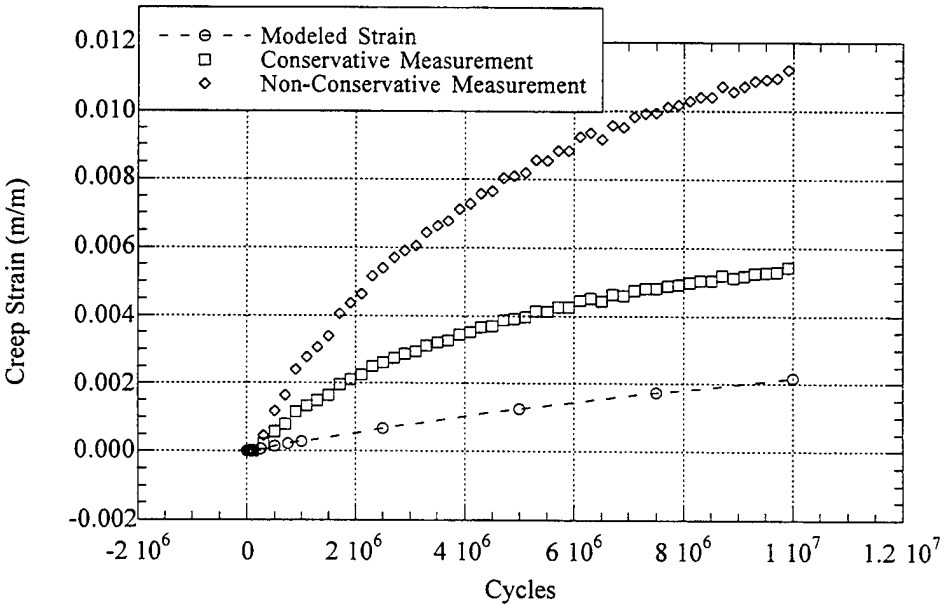

b) 400 Hz

Figure 4-16. Theoretical vs. Experimental Strain

(R = 0.8, 975 MPa - second loading block)

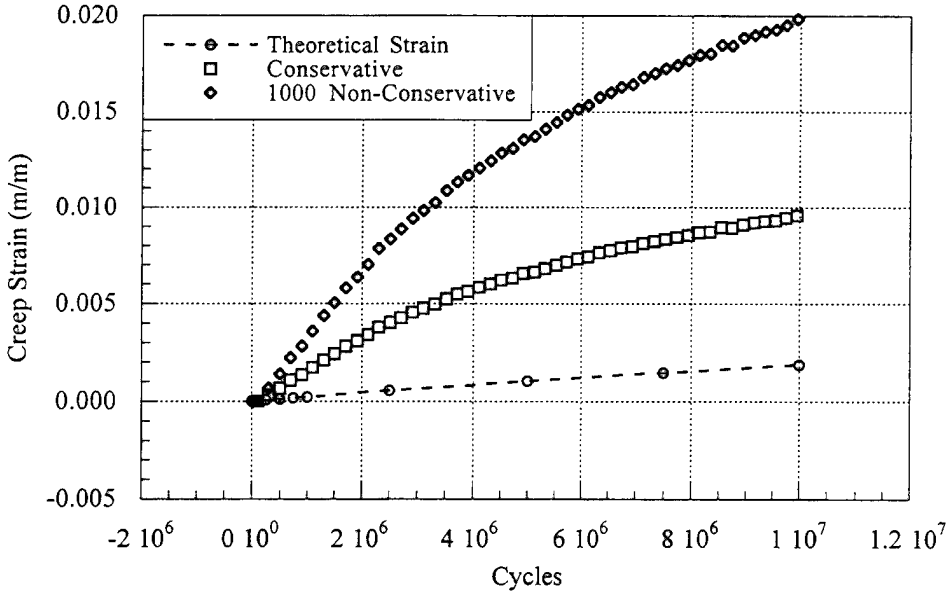

a) 70 Hz

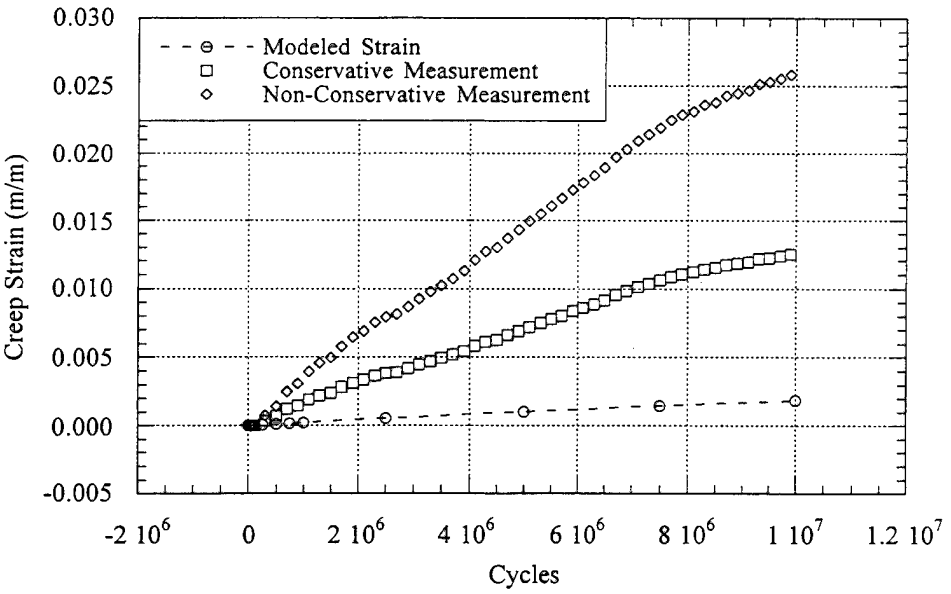

b) 400 Hz

Figure 4-17. Theoretical vs. Experimental Strain

(R = 0.8, 1000 MPa - third loading block)

Part of the disparity between the model and the experimental data may be due to the way in which the model accounts for cyclic loading. A linear summation of creep strain is assumed, and may not be a valid representation of time-dependent deformation under variable loading. The actual material response depends on prior load history, which is not accounted for in the model.

It is also apparent that differences occur between specimens at the different frequencies. Specimens tested at 70 Hz exhibited more than 1.5 times the amount of cumulative strain as those tested at 400 Hz. This is expected since the loading block takes much longer to complete, and agrees with the assumption of time dependency in strain accumulation during fatigue loading.

Cyclic Ratchetting

The results of the creep modeling seem to indicate that a second mechanism is at least partly responsible for the strain accumulation during HCF in Ti-6Al-4V. The theoretical predictions of the creep response greatly underestimate the actual strains. In addition, strain accumulation throughout the life of the specimen seems to be more a function of cycles than time. This can be seen clearly in Figures 4-18 and 4-19, which show the elongation versus time and elongation versus cycles relationships for two specimens at each frequency. The Figures clearly show the cycle dependence of strain accumulation.

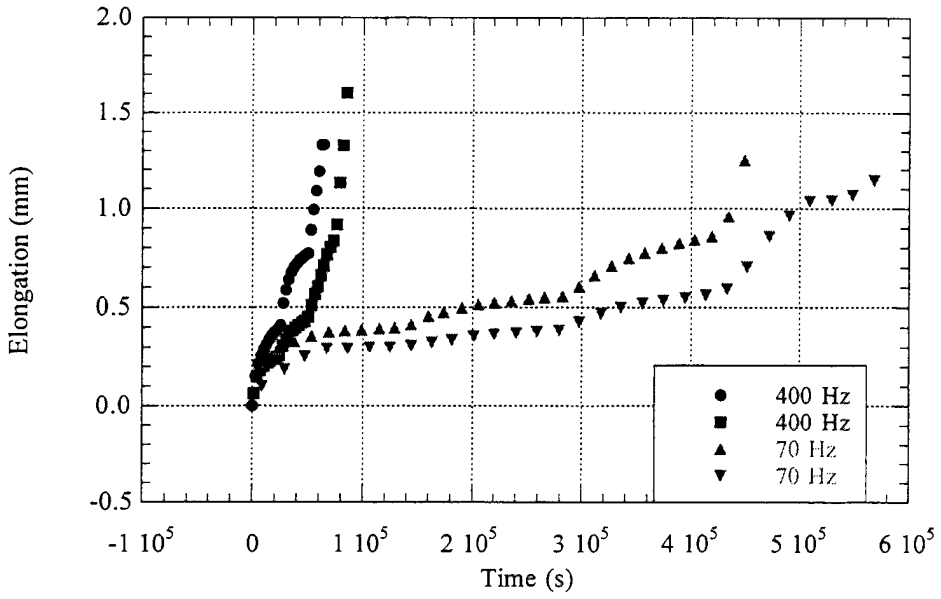

Figure 4-18. Specimen Elongation vs. Time

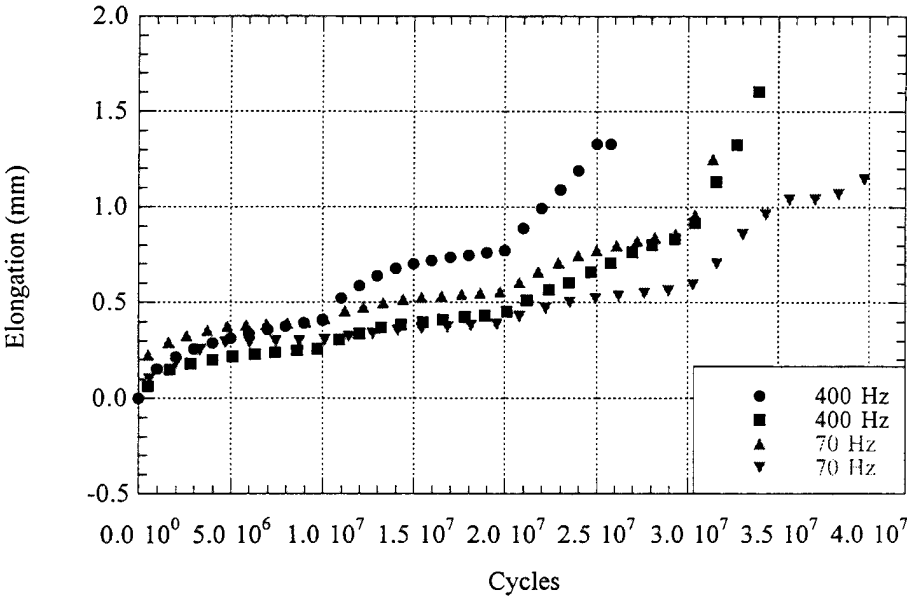

Figure 4-19. Specimen Elongation vs. Cycles

A possible explanation of these effects is ratchetting, a cycle-dependent accumulation of strain during cycling. The characteristic curves for this phenomenon are approximately the same shape as creep curves and those seen in this experiment for HCF loading. A sharp increase in strain is seen during the initial phase of the cycling, followed by a steady decrease in the strain rate as the number of cycles increases. Recent work on two rail steels [20] has shown success in modeling this behavior under complex loading conditions involving proportional and non-proportional loading at various stress ratios.

Another feature of the HCF failures at high stress ratios involves the strain accumulated at failure. The creep tests performed on this material showed a strain at failure slightly greater than 10 percent. This agrees with the strain to failure calculated using the gage section as the effective gage length. This could imply that HCF at high stress ratios may lend itself to prediction techniques based on strain to failure, in view the bulk damage in the form of void nucleation and growth.

4.4 Coaxing

The debate on the existence of a coaxing effect has been underway since the early 1950's. Coaxing involves increasing a material's fatigue strength by cycling at stresses slightly below the expected fatigue limit. After cycling, stresses are increased by a small amount and cycling is resumed. Results have differed widely, with some showing that coaxing produces extremely large increases in fatigue strength [37], while others claimed it

is statistically insignificant or nonexistent [38]. The truth seems to lie somewhere in-between, depending on the material. The dominating opinion on the cause of the coaxing is that it is somehow related to the susceptibility of the material to strain aging. If this is the case, then Ti-6Al-4V would not be expected to be affected.

Because of fatigue strength estimation scheme employed in this investigation, coaxing was a serious concern. Two steps were taken to eliminate this factor from consideration. First, all tests were begun at the same maximum stress for each stress ratio, regardless of frequency. In this way, if coaxing was present, all specimens would be subjected to exactly the same amount. As long as any coaxing taking place was not frequency dependent, the results could still be compared and evaluated. The second method for determining the coaxing effect involved performing some tests by starting at higher initial maximum stresses and comparing the fatigue strengths. These tests were performed at 1800 Hz, and preliminary data seem to indicate that a "reverse" coaxing effect is taking place at high mean stress. That is, specimens which first undergo cycling at lower stresses actually have lower fatigue strengths than specimens which start testing at higher stresses. This can be explained by the displacement results. It seems likely that plastic strain accumulation during a prior loading history would serve to damage the material and decrease the fatigue resistance. This is the scenario which is occurring due to the way in which tests were performed.

The basis for the fatigue limit estimation employed in this investigation assumes that no damage to the material occurs when cycling at a stress below the fatigue limit. Based on the results of the displacement and strain measurements taken during this study, it is apparent that this assumption is false at high stress ratios. Extensive deformation does occur during every loading block at these high mean stresses. This deformation at both frequencies helps to explain why similar fatigue strengths were found at a stress ratio of 0.8. Had fatigue strengths been determined for one type of loading cycle, so previous strain history could be neglected, the frequency effect may have been observed at high stress ratios. Based upon these findings, it seems that any "fatigue limit" determined at high stress ratios will be a function of the previous loading history.

CHAPTER V

CONCLUSIONS AND RECOMMENDATIONS

5.1 Conclusions

This study has shown that a frequency effect exists for Ti-6Al-4V tested under HCF conditions. Testing at higher frequencies results in a higher fatigue strength, or stress amplitude which will cause failure in 10^7 cycles. This effect occurs predominately at low stress ratios, and seems to disappear at stress ratios of approximately 0.8. This effect is important to designers of gas turbine engines, since most testing of materials is done at low frequencies while in-service applications may reach frequencies greater than 1 kHz.

The frequency dependence may be due to the interaction of several mechanisms. A few potential factors include strain rate effects on dislocation motion, diminished active primary slip systems at high frequencies in HCP and BCC materials, and environmental damage.

At high stress ratios, Ti-6Al-4V undergoes a change in fracture mode to a ductile failure, with no apparent single initiation and crack growth sites. This transition is

accompanied by a large amount of progressive strain accumulation during cycling and specimen necking at fracture, very similar to a standard tensile test.

An empirical model based on static creep test results did a relatively good job of predicting strain accumulation as a function of stress and time during the first loading block in HCF. However, the model severely underestimates the deformation on subsequent loading blocks.

An alternative explanation for the excessive plastic strain accumulation is cyclic ratchetting, which has been observed to exhibit strain accumulation similar to those in this study. Plots of cumulative strain versus time and strain versus cycles for specimens at different frequencies clearly show a cycle dependence, and the lack of correlation of time dependent creep after the initial loading block appears to support ratchetting as a primary mechanism.

The best explanation for the behavior of Ti-6Al-4V at high stress ratios most likely involves a combination of both of these phenomena, and possibly others as well. The results seem to indicate that creep may play an important role in the early stages, when primary creep is the dominating deformation process. At longer lives, however, the cycle dependence of the deformation becomes dominant.

Coaxing in Ti-6Al-4V does not increase the fatigue strength, as has been reported for some materials. On the contrary, previous loading seems to have a detrimental effect on the fatigue strength. At high stress ratios, this is likely due to the strain accumulation

during the initial loading blocks. This also suggest that ground-air-ground cycles, taken in combination with high frequency, high mean stress loading, may be much more damaging than if the low amplitude, high frequency cycles are absent.

5.2 Recommendations

The results of this investigation open the door to many possible avenues of future research:

A) An important aspect of this study involves the large accumulation of strain during high cycle fatigue at high mean loads. It has been suggested that room-temperature creep and cyclic ratchetting may account for this behavior. In order to more completely understand this phenomenon, a unified creep-plasticity model could be developed for this material. This would allow the prediction of the interaction of the α and β phases during the cyclic deformation, as well as any shakedown limits for ratchetting that arise from the two phase structure.

B) Another area of interest in gas turbine engine applications would be to simulate the effects of ground-air-ground cycles by introducing periodic underloads during HCF testing. The large strains seen during testing at

high mean stress and evidence of bulk damage indicate that such underloads may be very detrimental to the HCF resistance of the material.

C) Additional testing could also be performed at 1800 Hz to verify the results obtained thus far, especially at high stress ratios. An attempt should be made to understand the deviation of the 1800 Hz data from the 70 and 400 Hz data at a stress ratio of 0.8. One possible area to extend this research would be to extend the frequency testing to even lower frequencies to provide a larger range. This may not be feasible due to the extremely long tests which would be required.

D) The environmental effects on the frequency dependence could be determined by running tests in a vacuum and comparing the results to those obtained in air.

E) Creep tests could be performed with periodic changes to the load. The results of such experiments could then be compared to the static creep tests already performed at those loads to determine the material response under such conditions. This data could be used to develop a more accurate model to estimate the contribution of cyclic creep.

F) Extensometers could be used to develop hysteresis loops for the material, especially at low stress ratios where all plastic strain accumulation should

be caused by cyclic ratchetting. This may help to separate the effects of creep and ratchetting occurring at the high stress ratios.

G) Another important area, and a likely extension of this research, is to extend the high stress ratio testing to ratios approaching unity. This may help to understand and interpret the material response in this regime. Such research will be necessary if any constitutive modeling of the material's behavior is to be done. This modeling could extend some of the present work into the dual phase microstructure of Ti-6Al-4V. Modeling of this sort may require more extensive fractography at the pertaining stress ratios.

H) Some of the high stress ratio testing could also involve a closer look at the strain to failure in HCF. This, along with the previously mentioned testing, will require a more accurate measure of strain accumulation during the fatigue testing. This may prove to be very difficult due to the high frequencies involved.

I) Additional tests could also be performed to establish with certainty whether there is a coaxing effect in Ti-6Al-4V, and whether it is beneficial or detrimental to the fatigue strength.

APPENDIX A

TEST RESULTS

Nomenclature for Table A-1:

f:	frequency
R:	stress ratio
σmax initial:	maximum stress during first loading block
σmax prior:	maximum stress during loading block prior to the block in which failure occurred
σmax final:	maximum stress during the final loading block (in which failure occurs)
N (σ final):	number of cycles performed in the final loading block before the specimen failed
σG linear:	"Goodman" stress determined by a linear interpolation between the last two loading blocks based on the number of cycles during the final block
t (hours):	time elapsed during test

Table A-1. Specimen Test Results

Specimen	diameter	f (Hz)	R	σmax initial	σmax prior	σmax final	N (σ final)	σG linear	t (hours)
96-P64 (10)	4.7574 mm	400	0.8	950	978.5	1007.885	377,494	980	14.15
96-P66 (2)	4.7676 mm	400	0.8	950	978.5	1007.855	2,324,028	985	15.50
96-815 #1	4.7879 mm	400	0.8	950	978.5	1007.885	870,296	981	14.49
96-815 #2	4.7774 mm	70	0.8	978.5	978.5	978.5	1,640,209	979	6.51
96-815 #3	4.8006 mm	400	0.8	978.5	978.5	978.5	17,234	979	0.01
96-815 #4	4.7930 mm	400	0.8	978.5	978.5	978.5	3,742,755	979	2.60
97-301	3.8608 mm	400	0.8	950	950	978.5	4940000	964	10.38
97-302	3.8608 mm	400	0.5	800	860	880	952380	862	14.55
97-304	3.7846 mm	70	0.5	800	800	820	1280320	803	44.76
97-305	3.8100 mm	400	0.5	800	880	900	2703112	885	36.60
97-307	3.8100 mm	70	0.5	800	820	840	1831128	824	86.63
97-308	3.8354 mm	70	0.1	700	680	700	6152935	692	24.42
97-309	3.8354 mm	70	0.1	680	720	740	840010	722	122.38
97-A24	3.2029 mm	400	0.1	680	820	840	1561264	823	56.64
97-A25	3.1877 mm	400	0.1	680	760	780	6642176	773	32.39
97-A26	3.1801 mm	400	0.8	950	975	1000	5782680	989	17.90
97-A28	3.1775 mm	400	0.5	800	920	940	703856	921	49.10
97-A29	3.1115 mm	400	0.1	680	780	800	3893152	788	44.37
97-A30	3.1547 mm	400	0.8	950	1000	1025	4369044	1,011	23.87
97-A31	3.2233 mm	70	0.8	950	950	950	4124725	935	16.37
97-A32	3.1877 mm	70	0.8	925	1000	1025	266208	1,001	159.79
97-A33	3.1826 mm	70	0.8	950	1000	1025	1846356	1,005	126.37
97-A34	3.1902 mm	70	0.1	680	700	720	331500	701	80.68
97-A35	3.2080 mm	70	0.1	680	760	780	2547520	765	208.52
97-A36	2.5908 mm	70	0.5	800	820	840	5000000	830	99.21

APPENDIX B

CREEP MODEL DEVELOPMENT

The following figures show the creep test results for the various stresses, as well as the logarithmic fits used to model them. The strains shown are from 0.3 percent to 5 percent strain, which are the values used to model the creep.

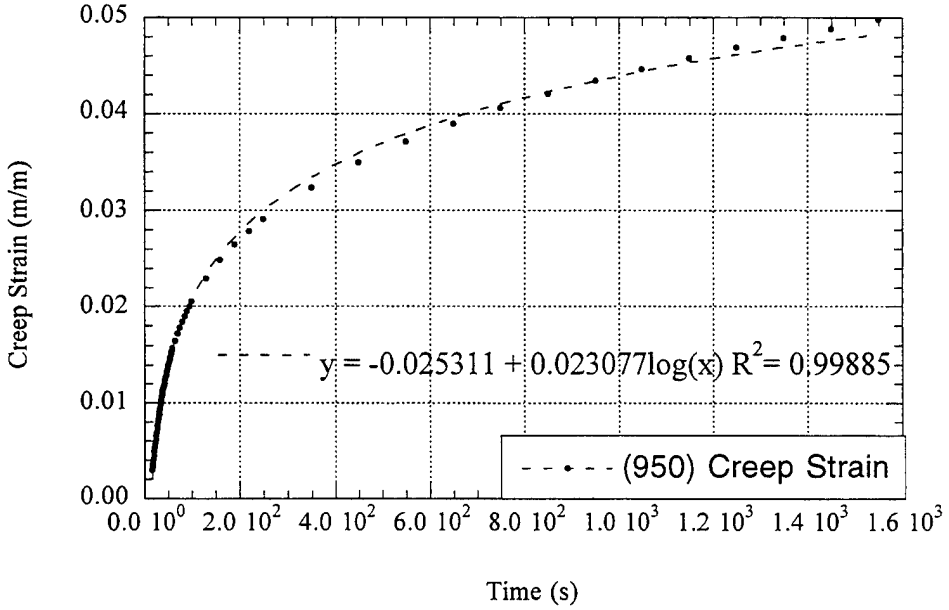

Figure B-1. Creep Strain vs. Time, 950 MPa

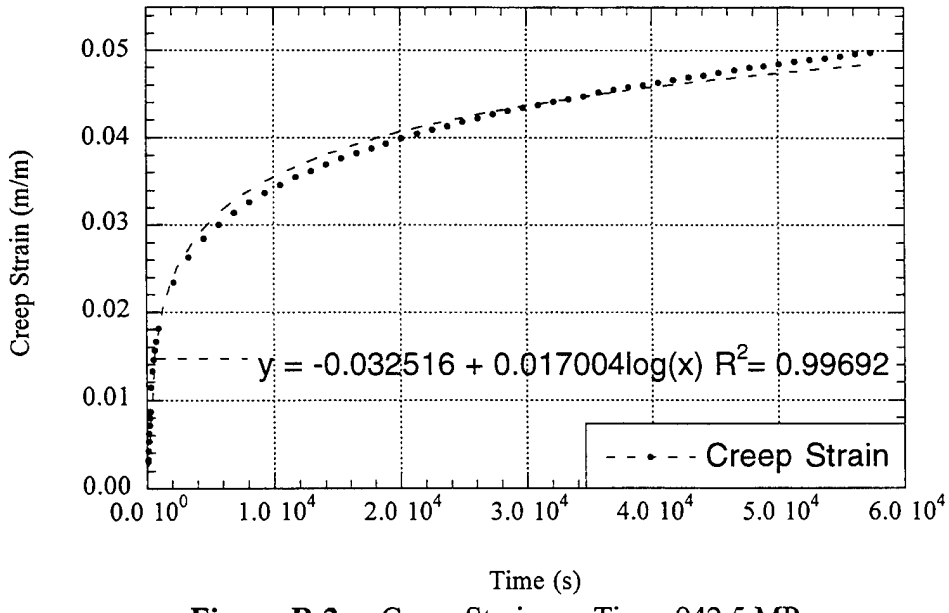

Figure B-2. Creep Strain vs. Time, 942.5 MPa

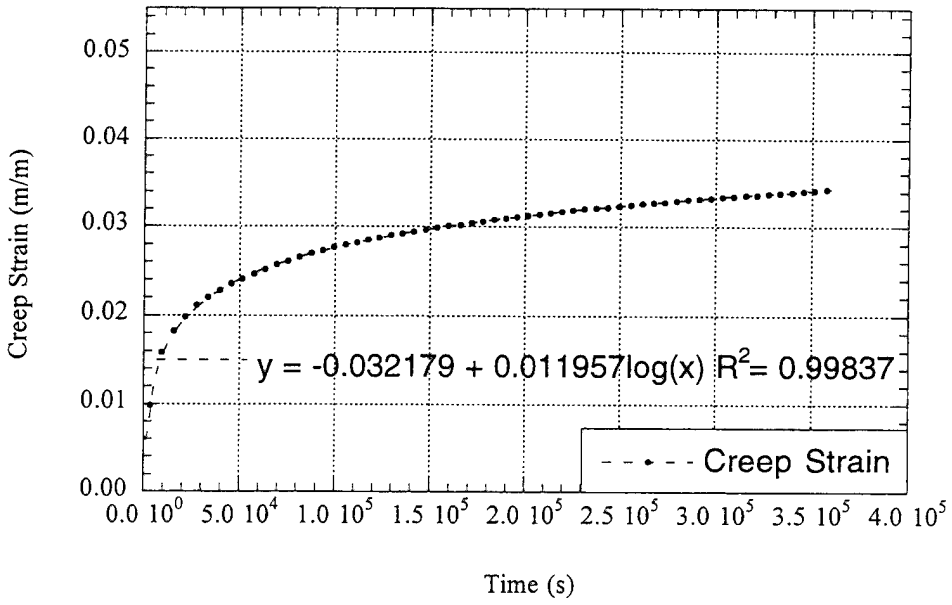

Figure B-3. Creep Strain vs. Time, 925 MPa

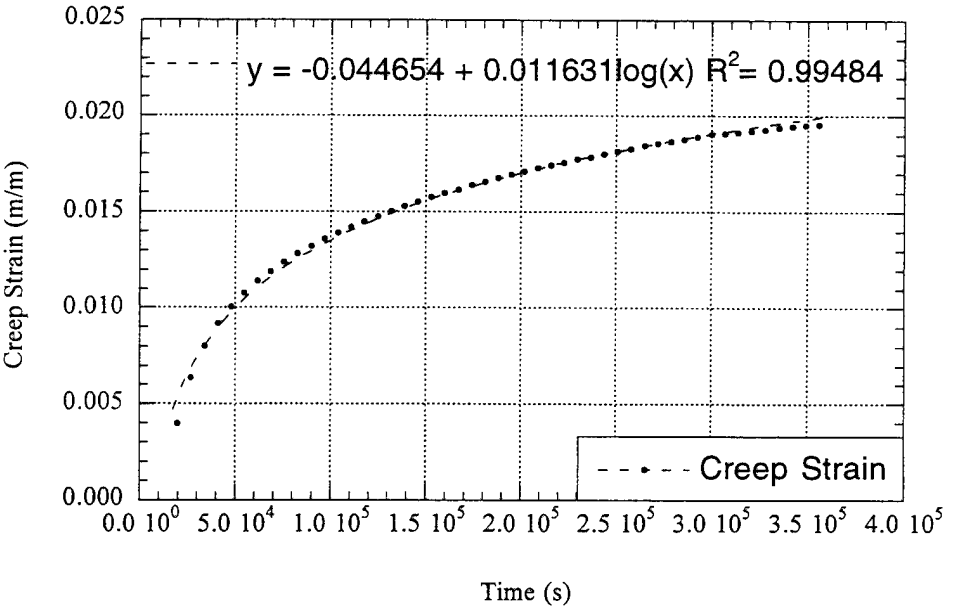

Figure B-4. Creep Strain vs. Time, 900 MPa

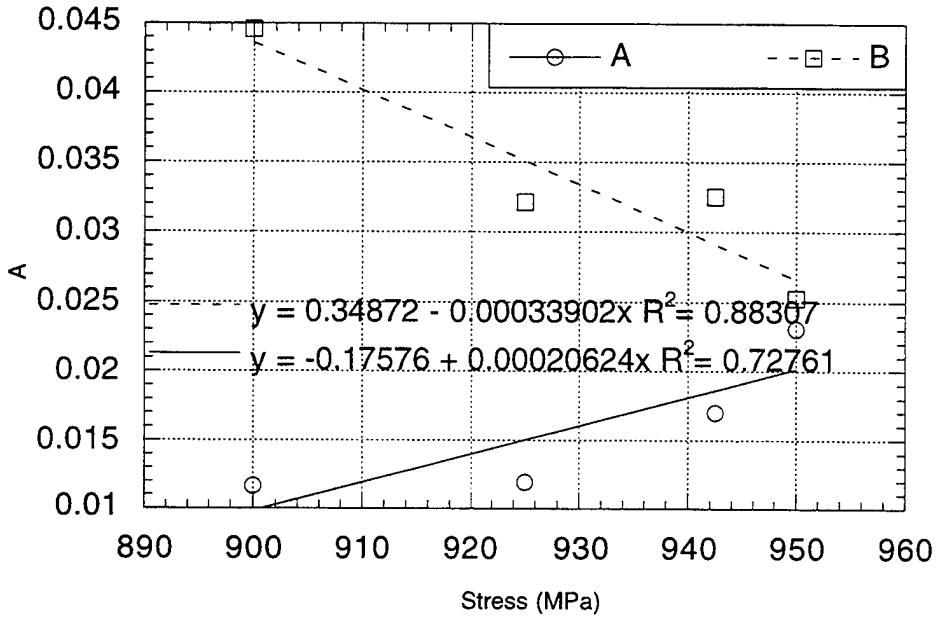

Figure B-5. Parameter Fit

Logarithmic creep curve fits were used to develop equations for strain as a function of time for each stress. They had the format:

$$\varepsilon^{c} = A \log(t) - B \tag{B.1}$$

The constants A and B are shown in Figures B.2 - B.6. They were plotted as a function of stress and a linear fit was used to develop equations of the form:

$$A = C_1 + C_2 \sigma \qquad B = C_3 + C_4 \sigma \tag{B.2}$$

The final equation for creep strain in terms of time and stress then became:

$$\varepsilon^{c} = (C_1 + C_2\,\sigma)\log(t) - (C_3 + C_4\,\sigma) \qquad \text{(B.3)}$$

This allowed the strain to be calculated for any value of stress and time. This equation was used for strains greater than 0.3 percent. For strains less than that value, a linear model was used. The linear equation used to model the initial creep behavior was of the form:

$$\varepsilon^{c} = \left(\frac{0.003}{t^{*}}\right) t \qquad \text{(B.4)}$$

where t* is the time required to reach a strain of 0.003 at any specified stress. The value of t* was found for any stress by solving equation B.3. Each cycle was then modeled as individual steps at various load levels. Figure B-1 shows the method used to break the cycle into parts.

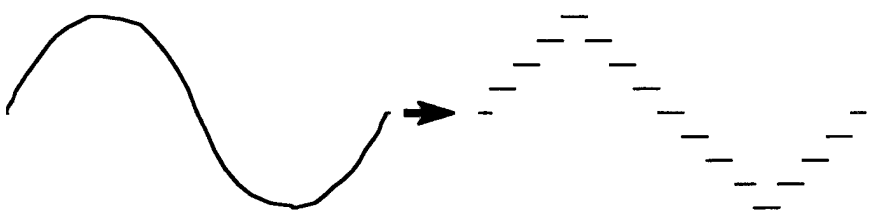

Figure B-6. Step Technique Used to Model Each Cycle

Table B-1. Empirical Constants Used for Creep Model

Constant	Value
C_1	-0.17576
C_2	2.06E-04
C_3	0.34872
C_4	-3.39E-04

The final creep model, as developed in Mathematica 3.0, is shown in Figure B-7 below. The version shown models the strain accumulated in the first 1000 cycles of a test with maximum stress of 975 MPa, R = 0.8. Each cycle is broken into 16 steps in this example. The resultant strain is listed as "p" in the model, and is shown on the last line. The nomenclature is as follows:

σ_M: maximum stress during a cycle

R: stress ratio

n: number of steps in the cycle

start: cycle number at which strain accumulation is begun

cycles: number of cycles during which strain accumulation is recorded

f: frequency of test being modeled

δT: duration of time spent at each step

STEP: amount of stress increase (or decrease) from one step to another

blocks: loading block during which cycling is modeled

```
σM = 975;
R = 0.8;
n = 16;
Start = 1;
Cycles = 100;
j = n Cycles;
f = 400;
δT = 1 / (f n);
STEP = 2 σM (1 − R) / n;
blocks = 1;
v = blocks * 10000000 / f;
A[σ_] := −0.17576 + 0.00020624 * σ;
B[σ_] := 0.34872 − 0.00033902 * σ;
ϵ[σ_, t_] := A[σ] Log[10, t] − B[σ];
σ = σM R + STEP;
z[x_] := 10^(B[x]+0.003)/(A[x]);
If[σ > 875,
 If[Start > 1,
  If[ϵ[σ, (Start / f + v) + δT] > 0.003,
   p = p + ϵ[σ, (Start / f + v) + δT] − ϵ[σ, (Start / f + v)], p = p + (0.003 / q) * δT],
  If[ϵ[σ, δT] > 0.003,
   p = p + ϵ[σ, δT],
   p = (0.003 / z[σ]) * δT]],
 p = 0];

For[i = 1, i ≤ (j − 1), i++,
 If[Mod[i, n] < (n / 2),
  σ = σ + STEP;
   If[σ > 875,
    If[ϵ[σ, (Start / f + v) + (i + 1) * δT] > 0.003,
     p = p + ϵ[σ, (Start / f + v) + (i + 1) * δT] − ϵ[σ, (Start / f + v) + i * δT],
          p = p + (0.003 / z[σ]) * δT],
    p = p],
  σ = σ − STEP;
   If[σ > 875,
    If[ϵ[σ, (Start / f + v) + (i + 1) * δT] > 0.003,
     p = p + ϵ[σ, (Start / f + v) + (i + 1) * δT] −
      ϵ[σ, (Start / f + v) + i * δT],
     p = p + (0.003 / z[σ]) * δT],
    p = p]]]
Print[p]

2.92314 × 10^−8
```

Figure B-7. Creep Model

REFERENCES

1. T. Nicholas and J.R. Zuiker, On the Use of the Goodman Diagram for High Cycle Fatigue Design, *International Journal of Fracture* 80 (1996) 219-235.

2. J.M. Larsen, B.D. Worth, C.G. Annis Jr. and F.K. Haake, An Assessment of the Role of Near-Threshold Crack Growth in High-Cycle-Fatigue Life Prediction of Aerospace Titanium Alloys Under Turbine Engine Spectra, *International Journal of Fracture* 80 (1996) 237-255.

3. T.D. Fett, D. Munz and G. Thun, Influence of Frequency on Cyclic Fatigue of Coarse Grained Al_2O_3, *Journal of Materials Science Letters* 12 (1993) 220-222.

4. H. Mayer and C. Laird, Influence of Cyclic Frequency on Strain Localization and Cyclic Deformation in Fatigue, *Materials Science and Engineering* 187(A) (1994) 23-35.

5. Z. Qian, S. Takezono and K. Tao, Effect of Loading Frequency on Fatigue Crack Growth Under High Temperature, *International Journal of Solids and Structures* 33(24) (1996) 3601-3610.

6. K. Makhlouf and J.W. Jones, Effects of Temperature and Frequency on Fatigue Crack Growth in 18% Cr Ferritic Stainless Steel, *International Journal of Fatigue* 15(3) (1993) 163-171.

7. I. Trockels, G. Lutjering and A. Gysler, Influence of Frequency of Fatigue Crack Propagation Behavior of Aluminum Alloys in Aggressive Environment, *Fatigue '96: Proceedings of the Sixth International Fatigue Congress*, Berlin, Germany (1996) 571-576.

8. C. Bathias and N. Jingang, Determination of Fatigue Limit Between 10^5 and 10^9 Cycles Using an Ultrasonic Fatigue Device, *Advances in Fatigue Lifetime Prediction Techniques: Second Volume*, ASTM STP 1211, ASTM, Philadelphia (1993) 141-152.

9. V.A. Kuz'menko, Fatigue Strength of Structural Materials at Sonic and Ultrasonic Loading Frequencies, *Ultrasonics* (1975) 21-30.

10. L.D. Roth, L.E. Willertz and T.R. Leax, On the Fatigue of Copper up to Ultrasonic Frequencies, *Proceedings of the First International Conference on Fatigue and Corrosion Fatigue up to Ultrasonic Frequencies,* Champion, PA (1981) 265-282.

11. X. Demulsant and J. Mendez, Influence of Environment on Low Cycle Fatigue Damage in Ti-6Al-4V and Ti 6246 Titanium Alloys, *Materials Science and Engineering* 219(A) (1996) 202-211.

12. M. Peters, A. Gysler and G. Lutjering, Influence of Texture on Fatigue Properties of Ti-6Al-4V, *Metallurgical Transactions* 15(A) (1984) 1597-1605.

13. H. Ghonem and R. Foerch, Frequency Effects on Fatigue Crack Growth Behavior in a Near-α Titanium Alloy, *Materials Science and Engineering* 138(A) (1991) 69-81.

14. S. Adachi, L. Wagner and G. Luetjering, Influence of Mean Stress on Fatigue Strength of Ti-6Al-4V, *Proceedings of the 7th International Conference on the Strength of Metals and Alloys* (ICSMA 7) (1986) 2117-2122.

15. S. Adachi, L. Wagner and G. Luetjering, Influence of Mean Stress on Fatigue Crack Nucleation in (α+β) Titanium Alloys, *International Conference of Fatigue of Engineering Materials and Structures*, London, IMechE Conference Publications 1986-9 (1986) 67-74.

16. F. Lorenzo and C. Laird, Cyclic Creep Acceleration and Retardation in Polycrystalline Copper Tested at Ambient Temperature, *Acta Metallurgica* 32(5) (1984) 681-692.

17. P. Lukas and L. Kunz, Effect of Mean Stress on Cyclic Stress-Strain Response and High Cycle Fatigue Life, *International Journal of Fatigue* 11(1) (1989) 55-58.

18. C.M. Gilmore and M.A. Imam, Static and Cyclic Creep Properties of Ti-6Al-4V for Several Heat Treatments, Institute for the Study of Fatigue, Fracture and Structural Reliability, ONR, Arlington (1975) 25p.

19. W.J. Evans, Creep-Fatigue Interactions in Ti-6Al-4V at Ambient Temperatures, *Third International Conference on Creep and Fracture of Engineering Materials*, Swansea, UK (1987) 603-613.

20. D.L. McDowell, Stress State Dependence of Cyclic Ratchetting Behavior of Two Rail Steels, *International Journal of Plasticity* 11(4) (1995) 397-421.

21. N. Ohno and J.-D. Wang, Kinematic Hardening Rules With Critical State of Dynamic Recovery, Part I: Formulation and Basic Features for Ratchetting Behavior, *International Journal of Plasticity* 9(3) (1993) 375-390.

22. N. Ohno and J.-D. Wang, Kinematic Hardening Rules With Critical State of Dynamic Recovery, Part II: Application to Experiments of Ratchetting Behavior, *International Journal of Plasticity* 9(3) (1993) 391-403.

23. Y. Jiang and H. Sehitoglu, Modeling of Cyclic Ratchetting Plasticity, Part I: Development of Constitutive Relations, *Journal of Applied Mechanics* 63(3) (1996) 720-725.

24. W.H. Reimann, Room Temperature Creep in Ti-6Al-4V, *Journal of Materials* 6(4) (1971) 926-940.

25. B.C. Odegard and A.W. Thompson, Low Temperature Creep of Ti-6Al-4V, *Metallurgical Transactions* 5 (1974) 1207-1213.

26. B.C. Odegard and R.E. Maringer, The Room Temperature Creep Behavior of Wrought and As-Welded Ti-6Al-4, Sandia Labs. Technical Report (1971).

27. G.Y. Gao and S.C. Dexter, Effect of Hydrogen on Creep Behavior of Ti-6Al-4V Alloy at Room Temperature, *Metallurgical Transactions* 18(A) (1987) 1125-1130.

28. K. Drefahl, P. Wincierz, U. Zwicker and P. Delarbre, 230000 h Creep Properties of Titanium Produced from Electrolytic and Sponge Material and Ti-6Al-4V Alloy at 20°C, *Titanium Science and Technology* 4 (1985) 2387-2394.

29. Z.A. Yang and Z.G. Wang, Effect of Frequency on Cyclic Creep of Polycrystalline Aluminum at Room Temperature, *Materials Science and Engineering* 142(A) (1991) 25-33.

30. W.J. Evans, Stress Relaxation and Notch Fatigue in Ti-6Al-4V, *Scripta Metallurgica* 21(9) (1987) 1223-1227.

31. ASM Handbook, Volume 19, *Fatigue and Fracture*, ASM International, Materials Park (1996).

32. D.C. Maxwell and T. Nicholas, A Rapid Method for Generation of a Haigh Diagram for High Cycle Fatigue, *Fatigue and Fracture Mechanics: 29th Volume*, ASTM STP 1321, T.L. Panontin and S.D. Sheppard (eds.), American Society for Testing and Materials (1998) (submitted for publication).

33. G.A. Hartman and N.E. Ashbaugh, A Fracture Mechanics Test Automation System for a Basic Research Laboratory, *Applications of Automation Technology to Fatigue and Fracture Testing,* A.A. Braun, N.E. Ashbaugh and F.M. Smith (eds.), ASTM STP 1092, ASTM, Philadelphia (1990) 95-110.

34. T. Nicholas, Tensile Testing of Materials at High Rates of Strain, *Experimental Mechanics* 21(5) (1981) 177-185.

35. R.W. Evans and B. Wilshire, Primary and Secondary Creep Behavior, *Creep of Metals and Alloys*, D. McLean (ed.), Dotesios Printers Ltd, England (1985) 69-113.

36. J.A. Collins, Failure of Materials in Mechanical Design: Analysis, Prediction, Prevention, John Wiley & Sons, New York (1981)

37. G.M. Sinclair, An Investigation of the Coaxing Effect in Fatigue of Metals, *ASTM Proceedings* 52 (1952) 743-758.

38. E. Epremian and R.F. Mehl, A Statistical Interpretation of the Effect of Understressing on Fatigue Strength, ASTM STP 137 (1952) 58-69.